Supplementary Materials for:

Taking advantage of the coordinative behaviour of a tridentate Schiff base ligand towards Pd^{2+} and Cu^{2+}

Jesús Sanmartín-Matalobos [1,*], Matilde Fondo [1], Morteza Zarepour-Jevinani [1,2], and Ana M. García-Deibe [1]

*jesus.sanmartin@usc.es

Table of Contents ..... **pages**

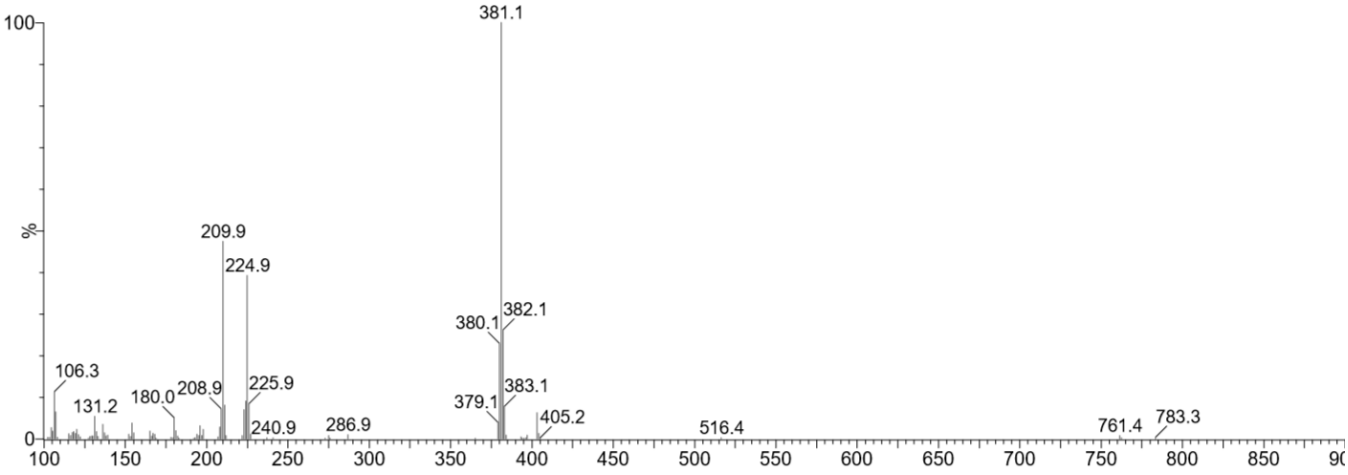

Figure S1. Partial view of the mass spectrum of H_2SB, showing the peak corresponding to $[H_2SB]^+$ (at about 381 *m*/*z*).

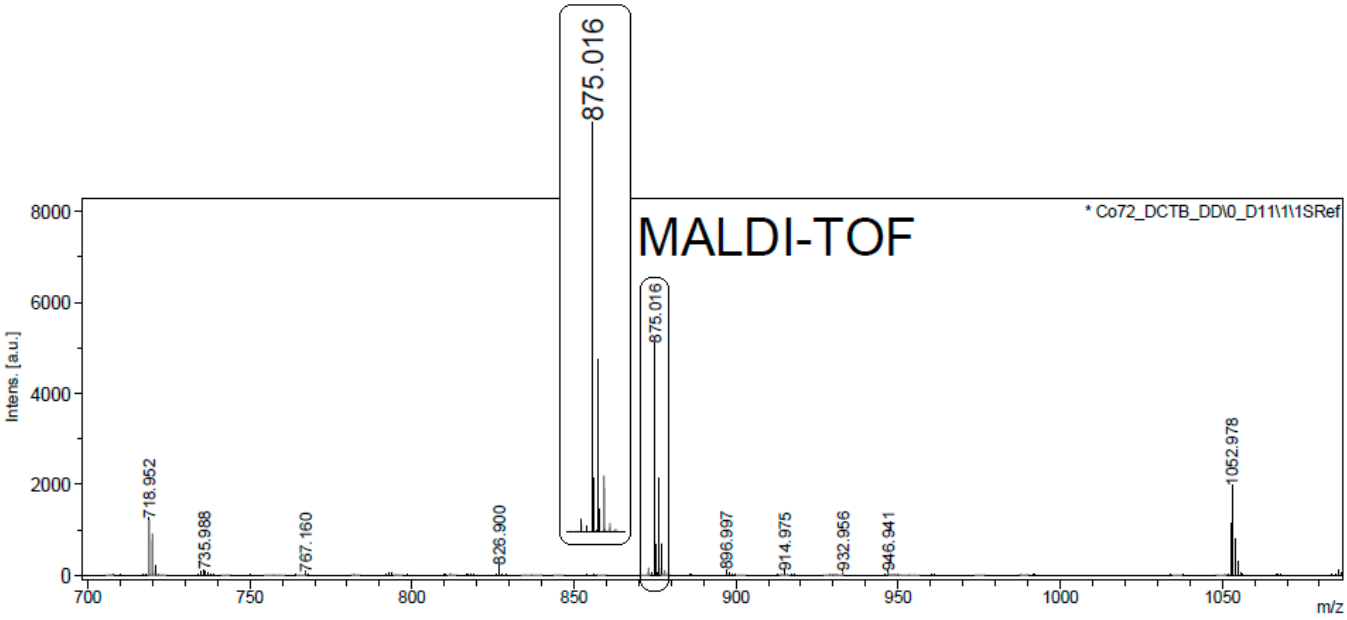

Figure S2. Partial view of the mass spectrum of $Co_2(SB)_2{\cdot}4H_2O$, showing the peak corresponding to $[Co_2(SB)_2]^+$ (at about 875 m/z).

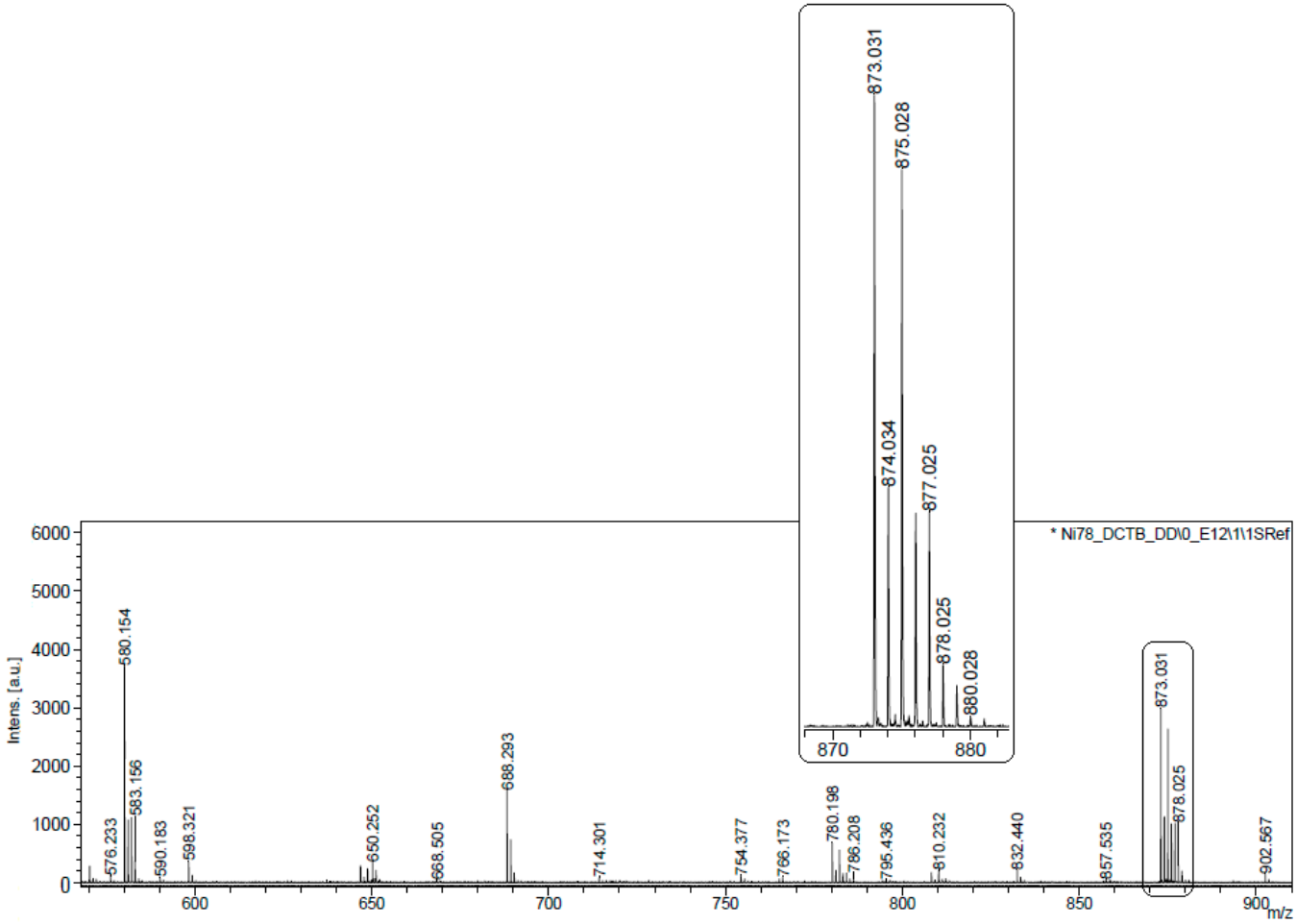

Figure. S3. Partial view of the mass spectrum of $Ni_2(SB)_2 \cdot 4H_2O$, showing the peak corresponding to $[Ni_2(SB)_2]^+$ (at about 875 m/z).

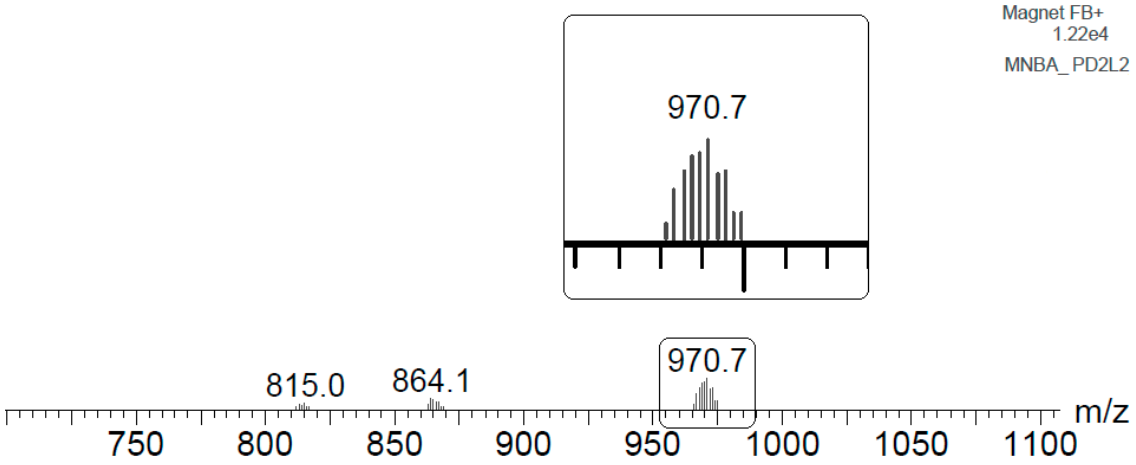

Figure S4. Partial view of the mass spectrum of $Pd_2(SB)_2$, showing the peak corresponding to $[Pd_2(SB)_2]^+$ (at about 971 m/z, amplified detail in box above.

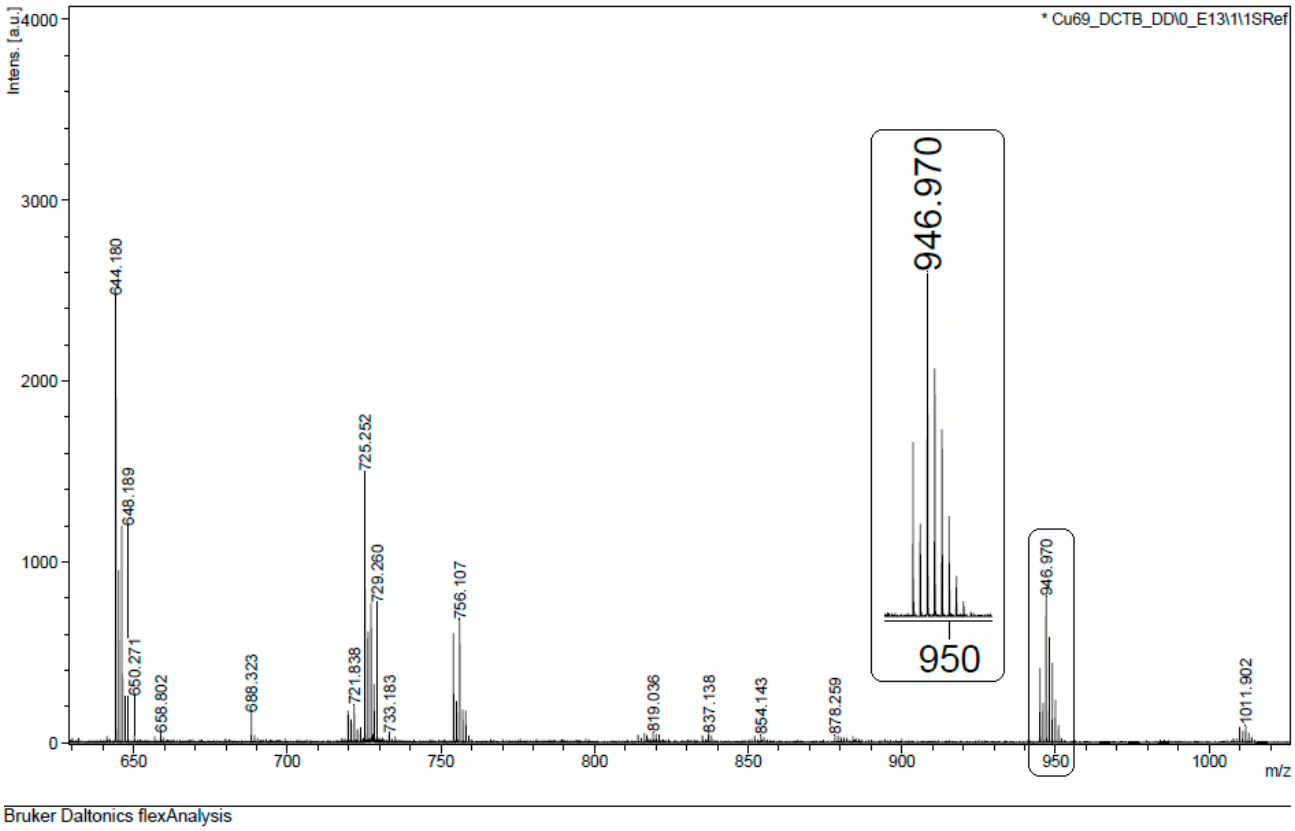

Figure S5. Partial view of the mass spectrum of $Cu_2(SB)_2 \cdot 2MeOH$, showing the peak corresponding to $[Cu_2(SB)_2(MeOH)_2]^+$ (at about 947 m/z).

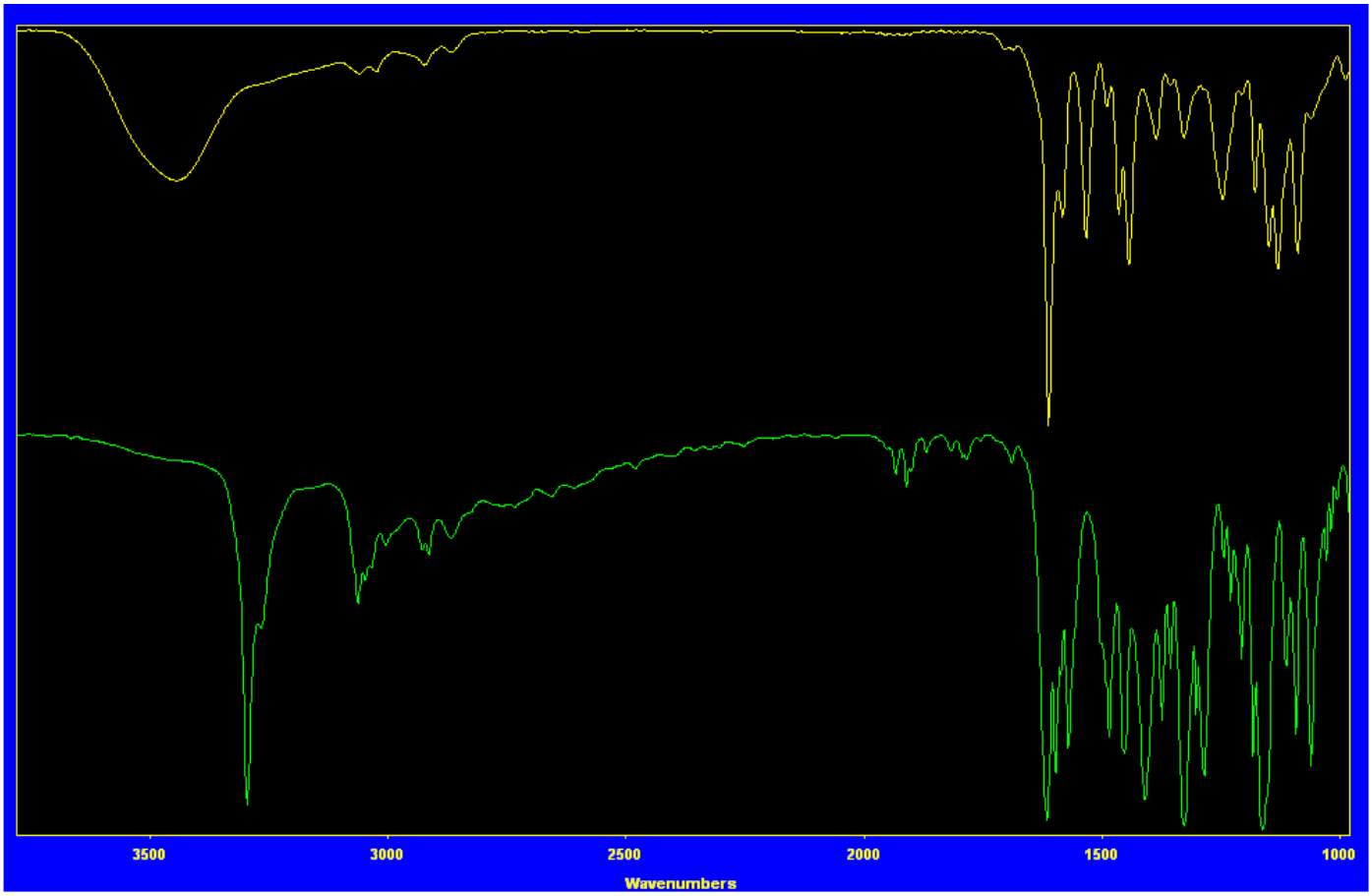

Figure S6. Partial view of the IR spectra of H_2SB (bottom) and $Cu_2(SB)_2{\cdot}2H_2O$ (top), showing the absence of both -OH (3296 cm^{-1}) and -NH- (3268 cm^{-1}) bands in the dinuclear complex.

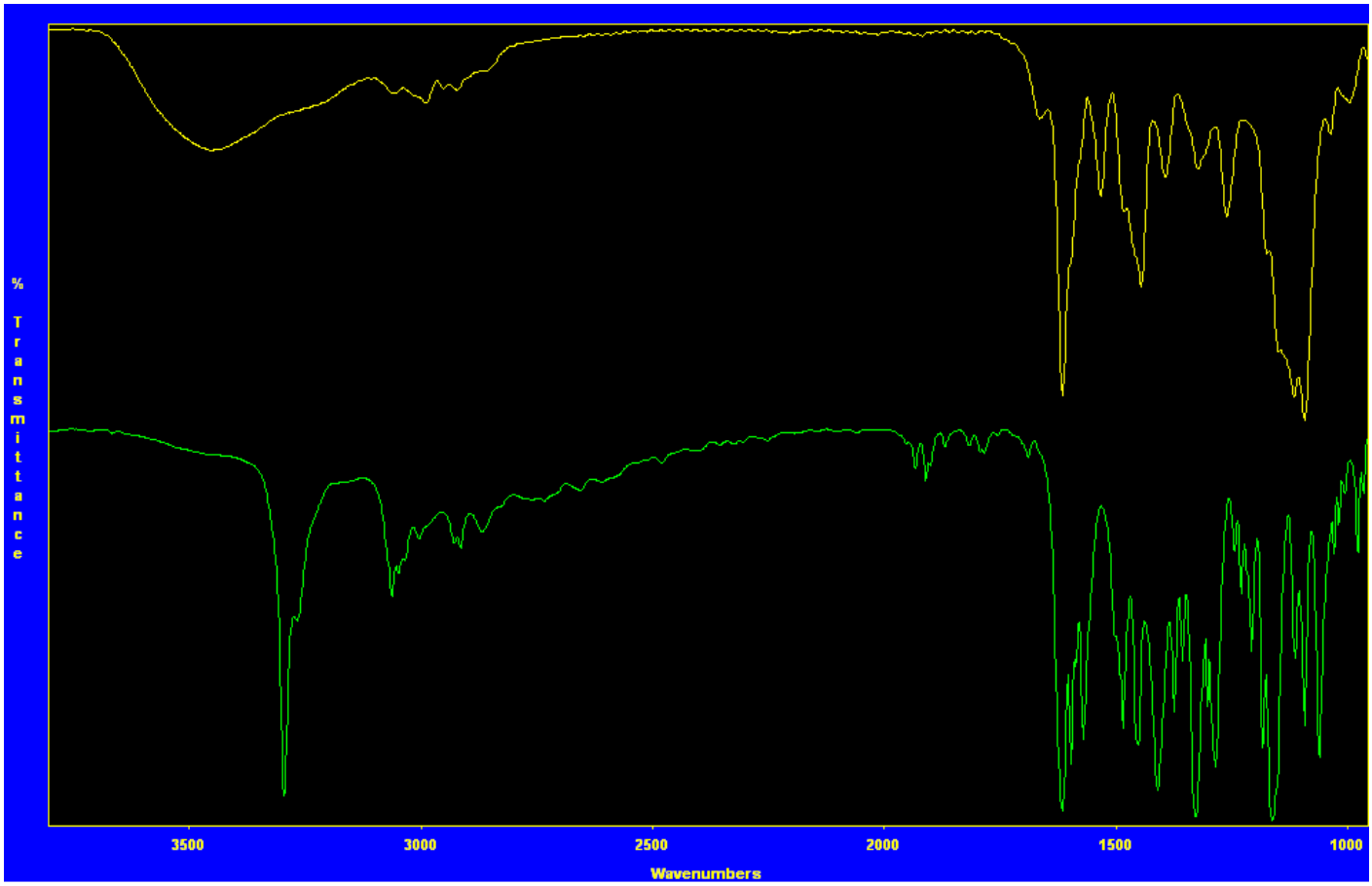

Figure S7. Partial view of the IR spectra of H_2SB (bottom) and $Zn_2(SB)_2 \cdot 4H_2O$ (top), showing the absence of both -OH (3296 cm^{-1}) and -NH- (3268 cm^{-1}) bands in the dinculear complex.

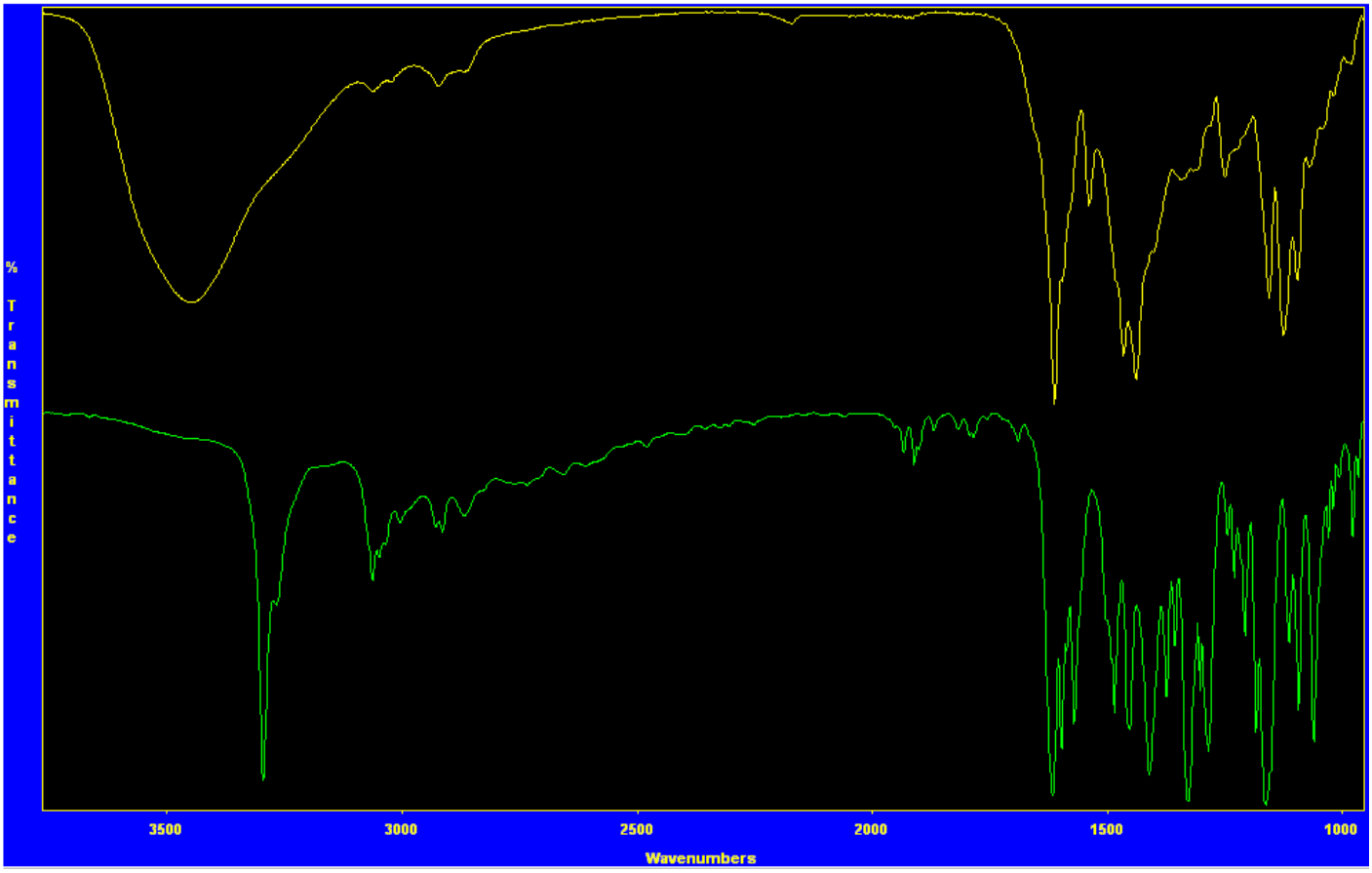

Figure S8. Partial view of the IR spectra of H_2SB (bottom) and $Cd_2(SB)_2$ (top), showing the absence of both -OH (3296 cm^{-1}) and -NH- (3268 cm^{-1}) bands in the dinuclear complex.

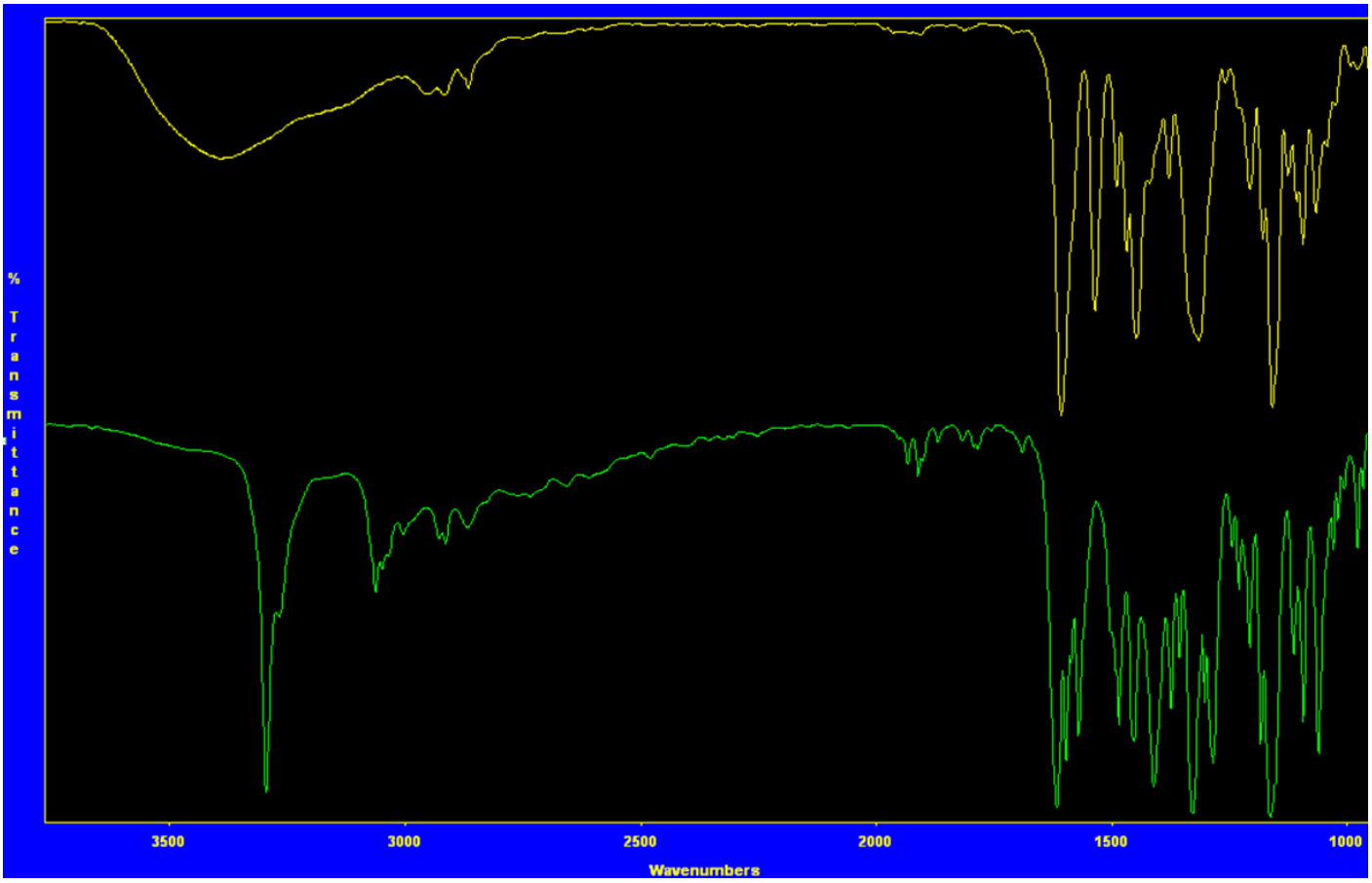

Figure S9. Partial view of the IR spectra of H_2SB (bottom) and $Ni_2(SB)_2{\cdot}4H_2O$ (top), showing the absence of both -OH (3296 cm^{-1}) and -NH- (3268 cm^{-1}) bands in the dinuclear complex.

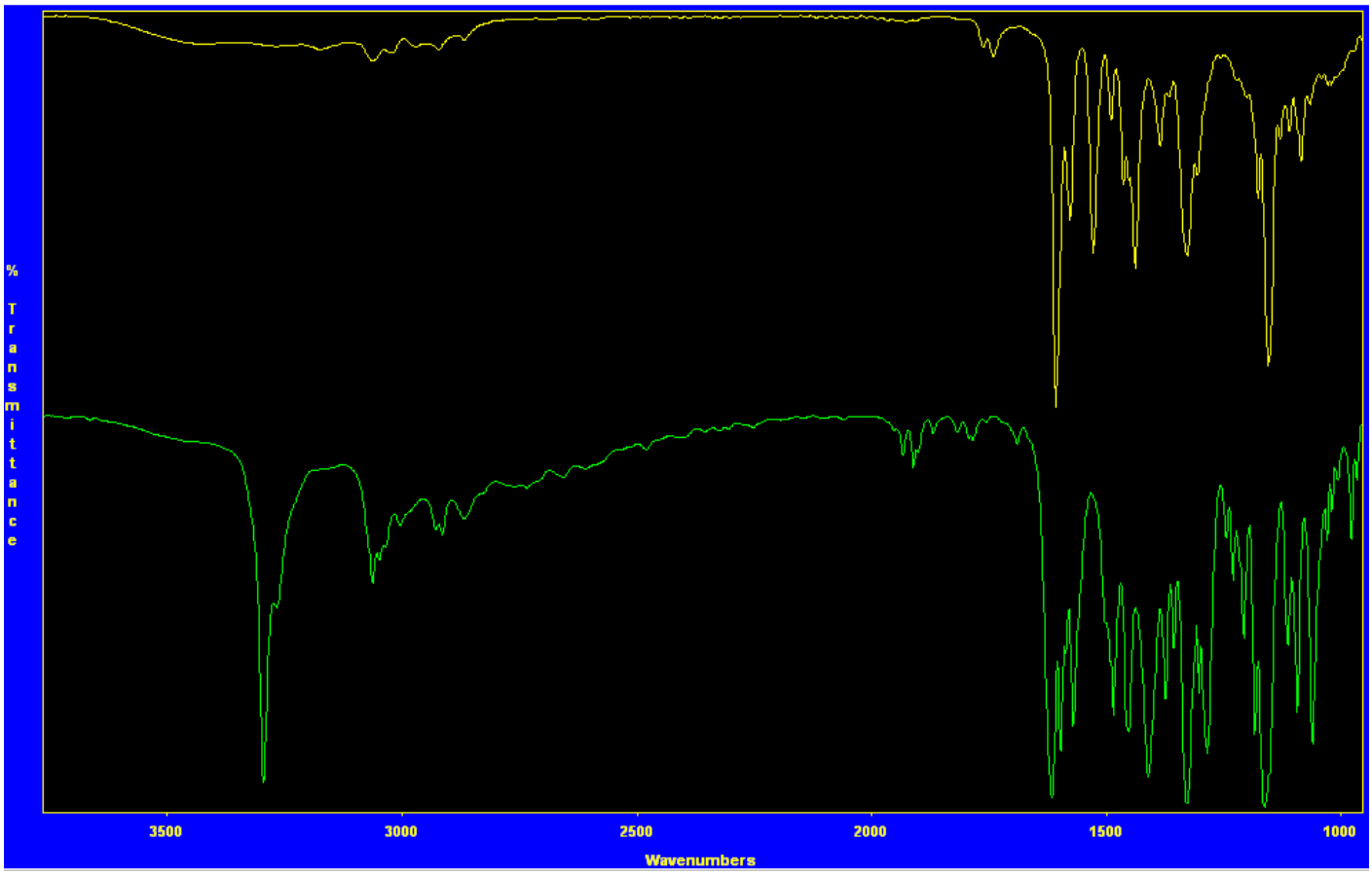

Figure S10. Partial view of the IR spectra of H_2SB (bottom) and $Pd_2(SB)_2$ (top), showing the absence of both -OH (3296 cm^{-1}) and -NH- (3268 cm^{-1}) bands in the dinuclear complex.

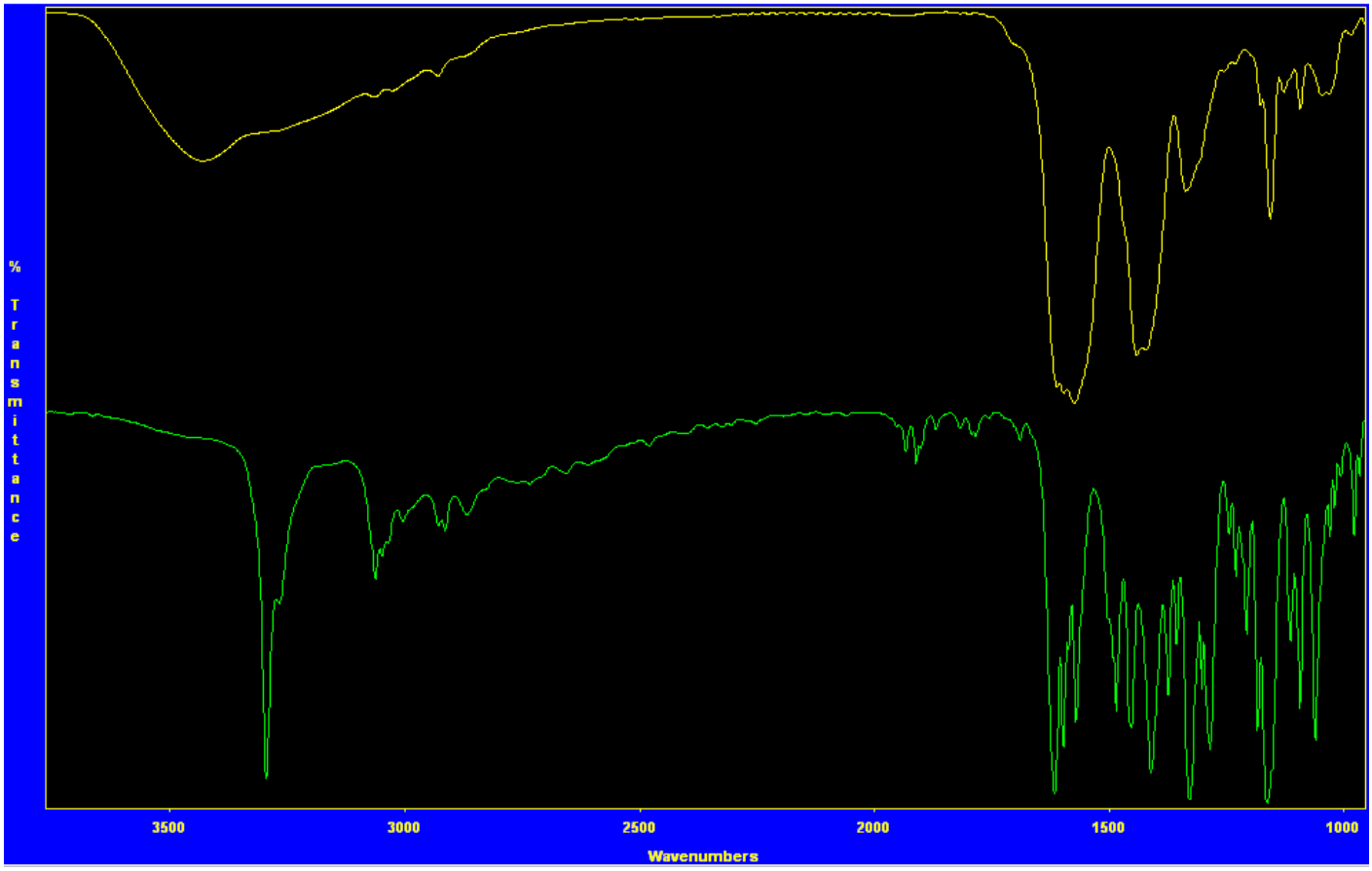

Figure S11. Partial view of the IR spectra of H_2SB (bottom) and $Co_2(SB)_2 \cdot 4H_2O$ (top), showing the absence of both -OH (3296 cm^{-1}) and -NH- (3268 cm^{-1}) bands in the dinuclear complex.

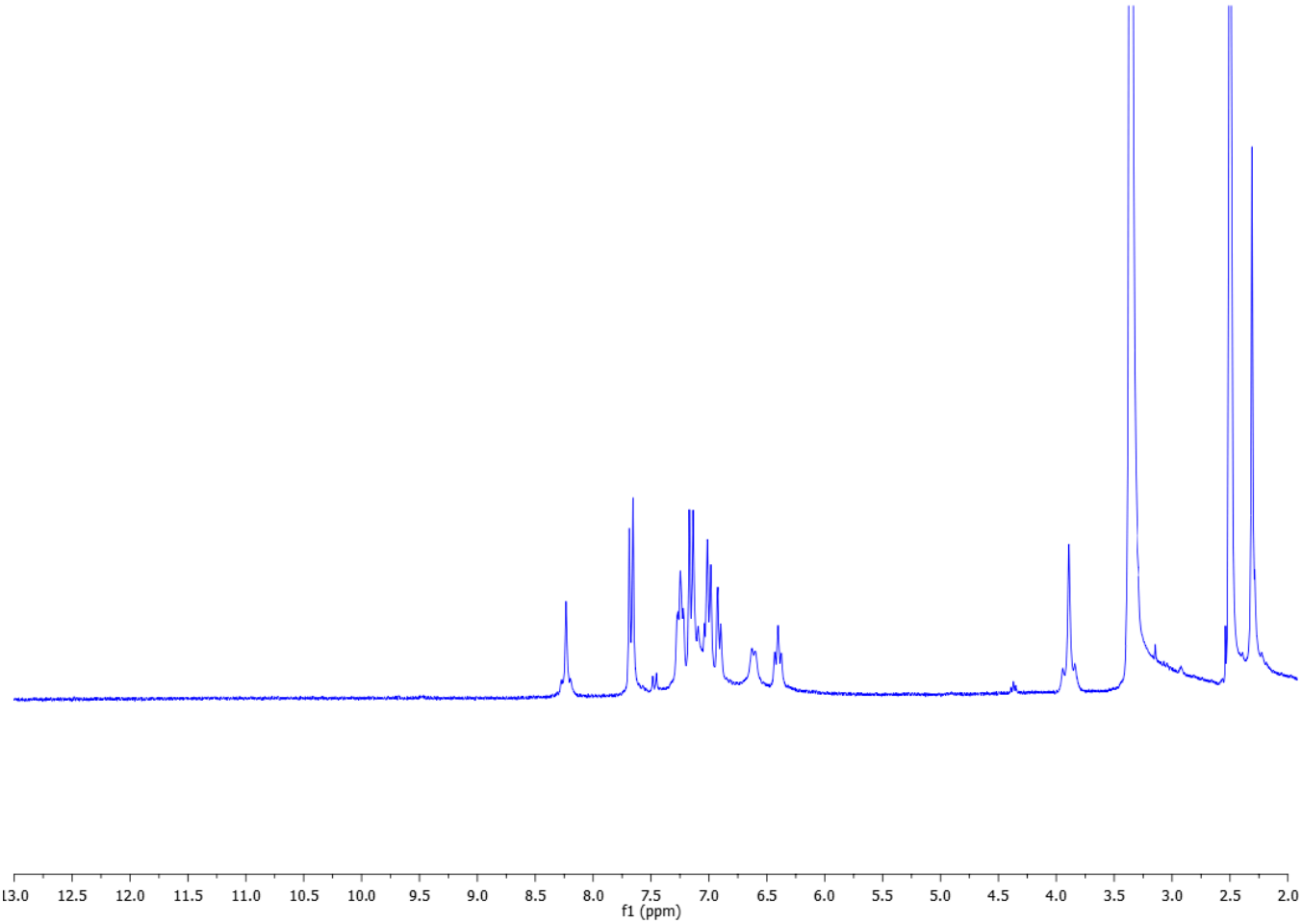

Figure S12. ^{1}H NMR spectrum of $Cd_2(SB)_2$, showing the absence of both -OH (12.5 ppm) and -NH- (8.0 ppm) signals in the dinuclear complex.

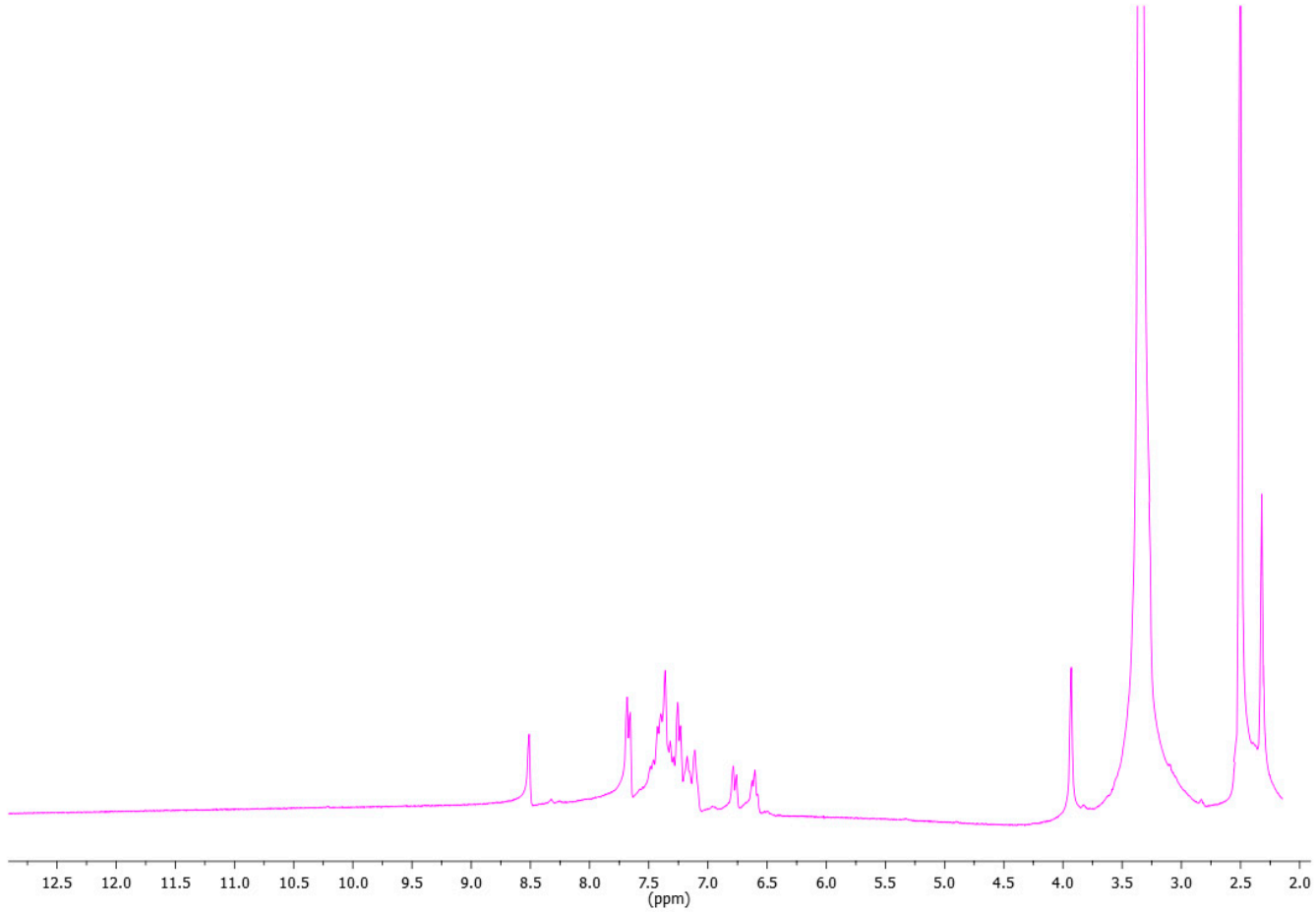

Figure S13. ^{1}H NMR spectra of $Zn_2(SB)_2{\cdot}4H_2O$, showing the absence of both -OH (12.5 ppm) and -NH- (8.0 ppm) signals in the dinuclear complex.

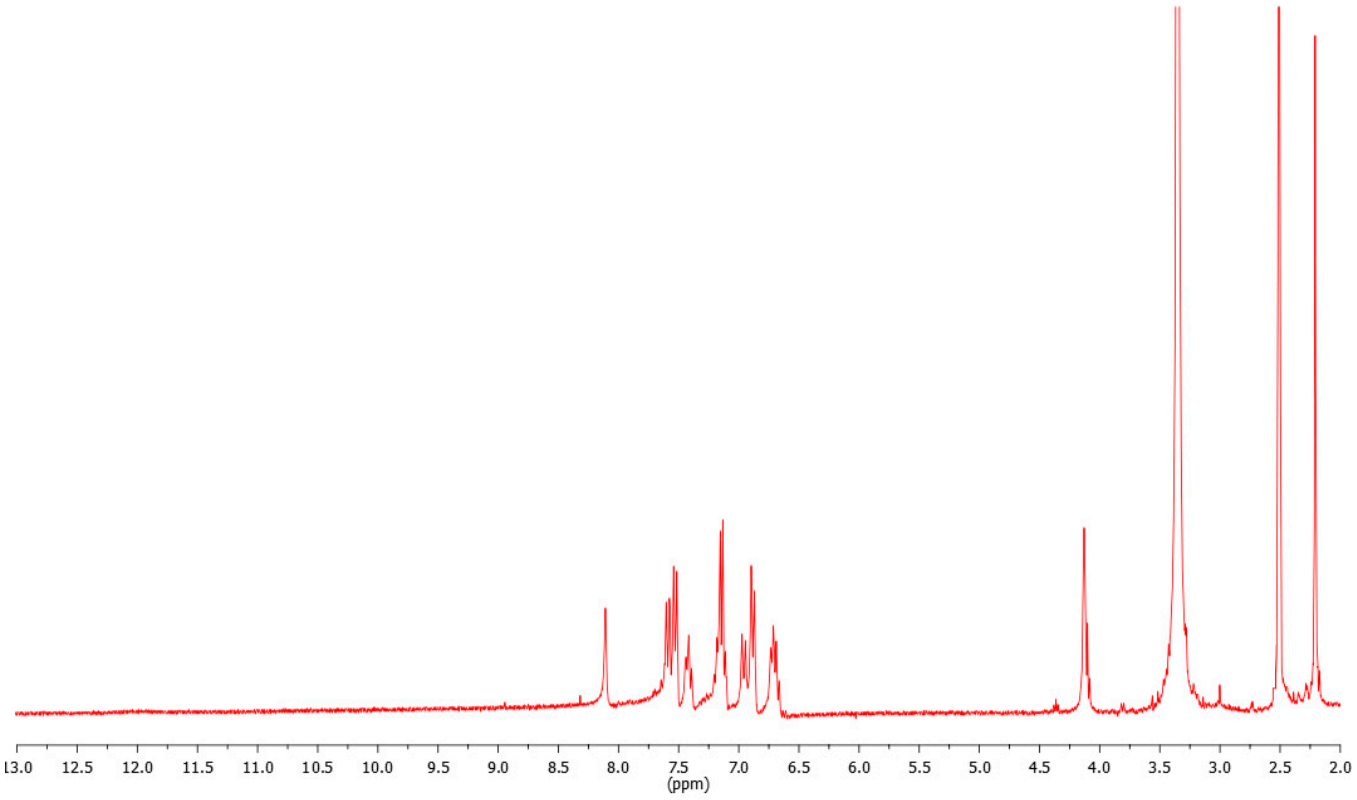

Figure S14. ^{1}H NMR spectra of $Pd_2(SB)_2$, showing the absence of both -OH (12.5 ppm) and -NH- (8.0 ppm) signals in the dinuclear complex.

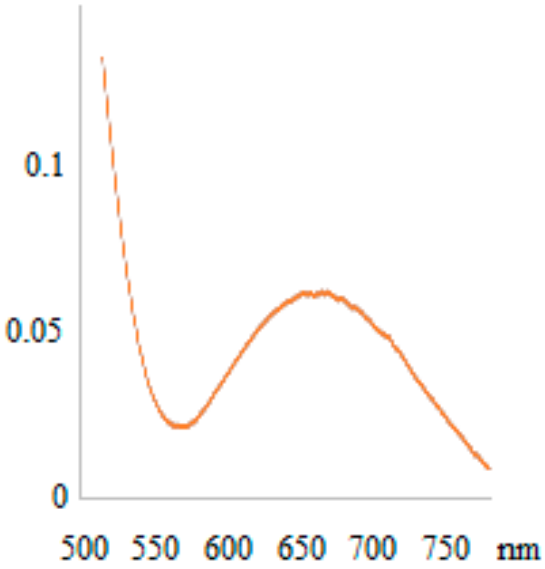

Figure S15. Partial view of the absorption spectrum of $Cu_2(SB)_2 \cdot 2MeOH$, showing the d-d transition.

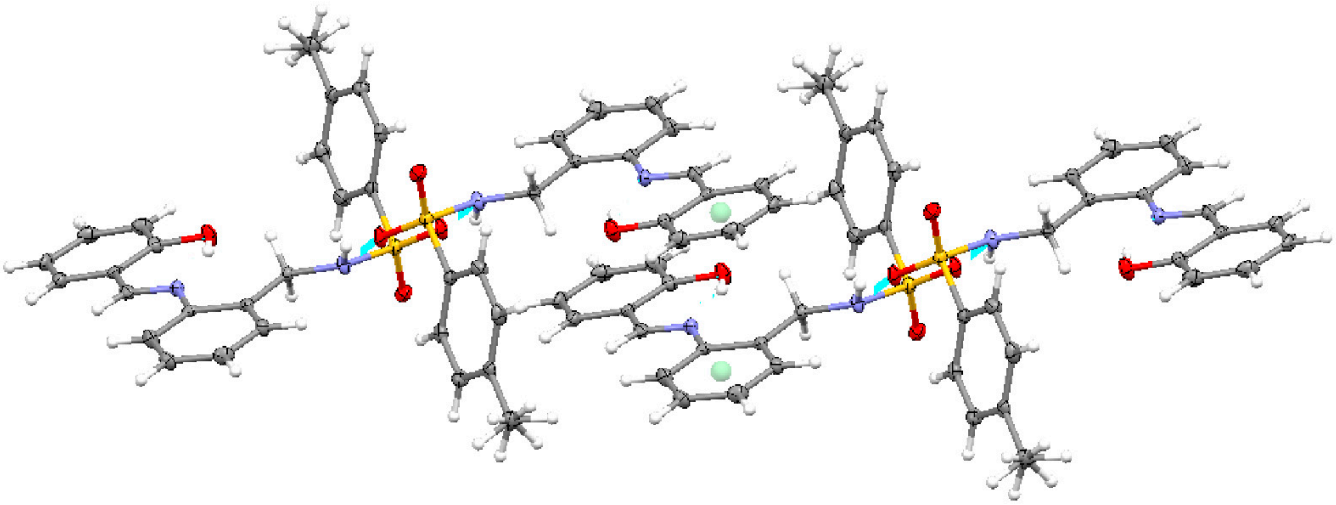

Figure S16. Two pairs of molecules of H_2SB, which are connected via H-bonds (light blue lines between donor and acceptor atoms) between neighbouring tosyl groups. At the same time, these pairs are consecutively π-π stacked with neighbouring pairs, being the distance between stacked rings (their centroids are represented in this figure as light green balls) of 3.77(2) Å.

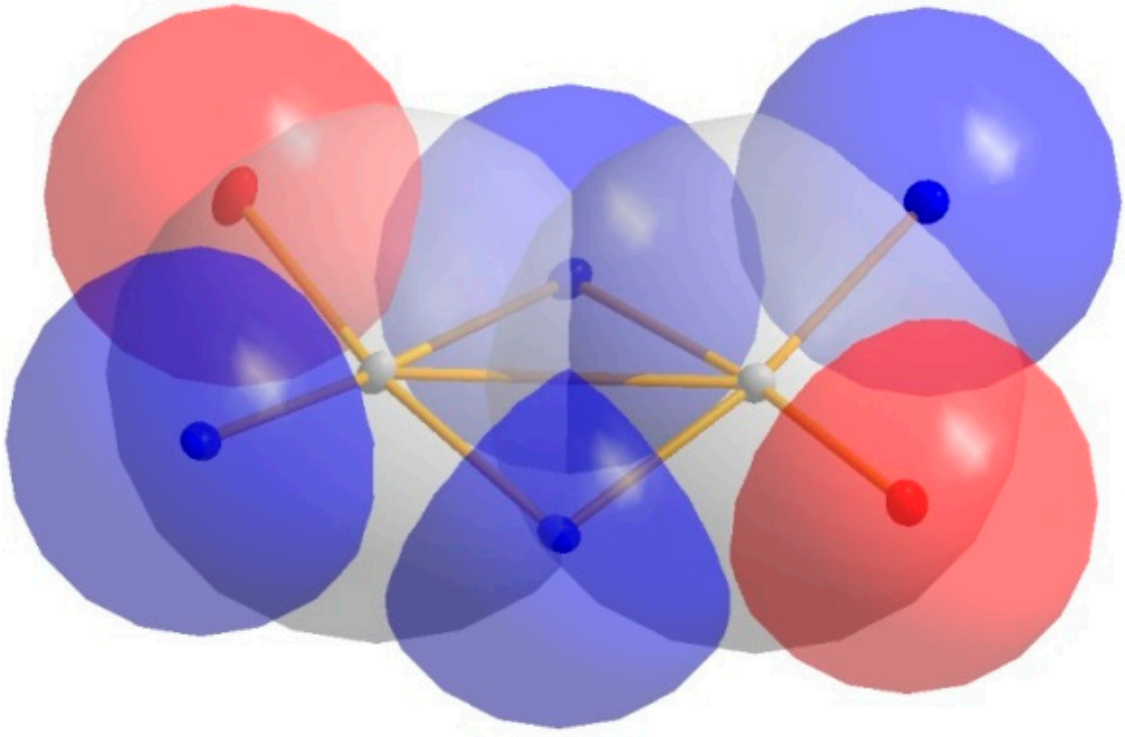

Figure S17. Superimposition of van der Waals radii and an ellipsoid scheme of the atoms constituting the two square-planar PdN2O2 coordination environments in Pd2(SB)2·Me2CO.

Table S1. Crystal data and structure refinement for H_2SB and $Pd_2(SB)_2{\cdot}Me_2CO$

Empirical formula	$C_{21}H_{20}N_2O_3S$	$C_{45}H_{42}N_4O_7Pd_2S_2$
Formula weight	380.45	1027.74
Crystal system	Triclinic	Monoclinic
Space group	*P* -1	$P2_1/c$
Unit cell dimensions	a = 7.4502(3) Å	a = 13.4356(2)
	b = 11.1160(5) Å	b = 13.4945(2)
	c = 11.7738(5) Å	c = 22.7123(4)
	α = 74.955(2)°.	α = 90
	β = 84.084(2)°.	β = 93.776(1)
	γ = 73.140(2)°.	γ = 90
Volume (Å^3)	900.76(7)	4108.95(11)
Z	2	4
Density (calculated, Mg/m^3)	1.403	1.661
Absorption coefficient (mm^{-1})	0.205	1.035
F(000)	400	2080
Crystal size (mm^3)	0.42 x 0.37 x 0.18	0.42 x 0.37 x 0.02
Theta range for data collection	1.792 to 26.018°	1.519 to 26.399
Index ranges	$-9 \le h \le 9$, $-12 \le k \le 13$, $0 \le l \le 14$	$16 \le h \le 16$, $0 \le k \le 16$, $0 \le l \le 28$
Reflections collected	15809	53054
Independent reflections	3544 (R_{int} = 0.0548)	8413 (R_{int} = 0.0668)
θ_{max} (Completeness to θ)	25.242° (99.8 %)	26.399 (100%)
Max. and min. transmission	1.0000 and 0.9387	1.0000 and 0.9089
Data / restraints / parameters	3544 / 0 / 253	8413 / 0 / 545
Goodness-of-fit on F^2	1.045	1.085
Final R indices [I > 2sigma(I)]	R_1 = 0.0536, wR_2 = 0.1023	R_1 = 0.0355, wR_2 = 0.0625
R indices (all data)	R_1 = 0.0848, wR_2 = 0.1169	R_1 = 0.0547, wR_2 = 0.0686
Largest diff. peak and hole (e.Å^{-3})	0.311 and -0.453	0.544 and -0.639

Table S2. Main bond distances [Å] and angles [°] for H_2SB

Atoms	**Distances**
C(1)-S(1)	1.767(3)
C(4)-C(40)	1.508(3)
C(5)-C(6)	1.378(3)
S(1)-O(2)	1.4312(17)
S(1)-O(1)	1.4378(18)
S(1)-N(1)	1.624(2)
N(1)-C(7)	1.462(3)
C(7)-C(8)	1.506(3)
C(8)-C(9)	1.394(4)
C(8)-C(13)	1.399(3)
C(13)-N(2)	1.422(3)
N(2)-C(14)	1.284(3)
C(20)-O(3)	1.350(3)
Atoms	**Angles**
C(2)-C(1)-S(1)	119.62(19)
C(6)-C(1)-S(1)	120.0(2)
C(5)-C(4)-C(40)	121.2(2)
C(3)-C(4)-C(40)	120.8(2)
O(2)-S(1)-O(1)	119.42(11)
O(2)-S(1)-N(1)	107.24(11)
O(1)-S(1)-N(1)	106.36(11)
N(1)-S(1)-C(1)	107.69(11)
C(7)-N(1)-S(1)	117.27(17)
N(1)-C(7)-C(8)	113.2(2)
C(8)-C(13)-N(2)	116.2(2)
C(12)-C(13)-N(2)	123.9(2)
C(14)-N(2)-C(13)	121.9(2)
N(2)-C(14)-C(15)	121.6(2)
N(2)-C(14)-H(14)	119.2
O(3)-C(20)-C(19)	118.5(2)
O(3)-C(20)-C(15)	121.6(2)
C(19)-C(20)-C(15)	119.9(2)
C(20)-O(3)-H(3H)	103(2)

Table S3. Classic hydrogen bonds for H_2SB [Å and °]

D-H...A	d(D-H)	d(H...A)	d(D...A)	<(DHA)
N(1)-H(1A)···O(1)$^{\#1}$	0.81(3)	2.27(3)	2.998(3)	149(2)
O(3)-H(3H)···N(2)	0.93(3)	1.74(3)	2.607(3)	155(3)

Symmetry transformations used to generate equivalent atoms:

$^{\#1}$ -x+1,-y,-z

Table S4. Main bond distances [Å] and angles [°] for $Pd_2(SB)_2 \cdot Me_2CO$

Atoms	Distance	Atoms	Distance
Pd1-O13	1.971(2)	Pd2-O23	1.972(2)
Pd1-N12	2.023(3)	Pd2-N22	2.022(3)
Pd1-N11	2.057(3)	Pd2-N21	2.058(3)
Pd1-N21	2.103(3)	Pd2-N11	2.090(3)
Pd1···Pd2	3.0102(4)		
C101-S11	1.766(3)	C201-S21	1.762(3)
N11-S11	1.693(3)	N21-S21	1.694(3)
N11-C107	1.501(4)	N21-C207	1.503(4)
C107-C108	1.499(5)	C207-C208	1.506(4)
C113-N12	1.442(4)	C213-N22	1.448(4)
N12-C114	1.308(4)	N22-C214	1.308(4)
C120-O13	1.299(4)	C220-O23	1.304(4)
Atoms	Angle	Atoms	Angle
O13-Pd1-N12	93.94(10)	O23-Pd2-N22	94.21(10)
O13-Pd1-N11	171.48(10)	O23-Pd2-N21	169.99(10)
N12-Pd1-N11	94.28(11)	N22-Pd2-N21	95.02(10)
O13-Pd1-N21	87.32(10)	O23-Pd2-N11	85.84(10)
N12-Pd1-N21	167.71(11)	N22-Pd2-N11	172.26(11)
N11-Pd1-N21	84.17(10)	N21-Pd2-N11	84.49(10)
C101-S11-N11	118.74(15)	C201-S21-N21	106.60(15)
C107-N11-S11	111.6(2)	C207-N21-S21	112.2(2)
O11-S11-O12	118.74(15)	O21-S21-O22	118.91(14)
N11-C107-C108	112.4(3)	N21-C207-C208	113.4(3)
N12-C114-C115	128.7(3)	N22-C214-C215	128.8(3)
C113-N12-C114	116.8(3)	C213-N22-C214	116.7(3)
O13-C120-C115	124.9(3)	O23-C220-C215	124.4(3)
Atoms	Torsion	Atoms	Torsion
S11-N11-C107-C108	-64.8(3)	S21-N21-C207-C208	-64.8(3)
N11-C107-C108-C113	-56.7(4)	N21-C207-C208-C213	-51.6(4)
C107-C108-C113-N12	-1.0(5)	C207-C208-C213-N22	-2.1(5)
C113-N12-C114-C115	-171.9(3)	C213-N22-C214-C215	-175.1(3)
C114-C115-C120-O13	-4.7(5)	C214-C215-C220-O23	-1.7(5)

Table S5. Hydrogen bonds for $Pd_2(SB)_2 \cdot Me_2CO$ [Å and °].

D-H···A	d(D-H)	d(H···A)	d(D···A)	<(DHA)
C(102)-H(102)···O(21)	0.95	2.29	3.214(4)	164
C(107)-H(10A)···O(201)	0.99	2.41	2.899(4)	110
C(202)-H(202)···O(10)	0.95	2.37	3.277(4)	160
C(207)-H(20B)···O(101)	0.99	2.49	2.980(4)	110

C(212)-H(212)···O(10)#1	0.95	2.48	3.243(4)	137

Symmetry transformations used to generate equivalent atoms:
#1 -x+1,y-1/2,-z+1/2

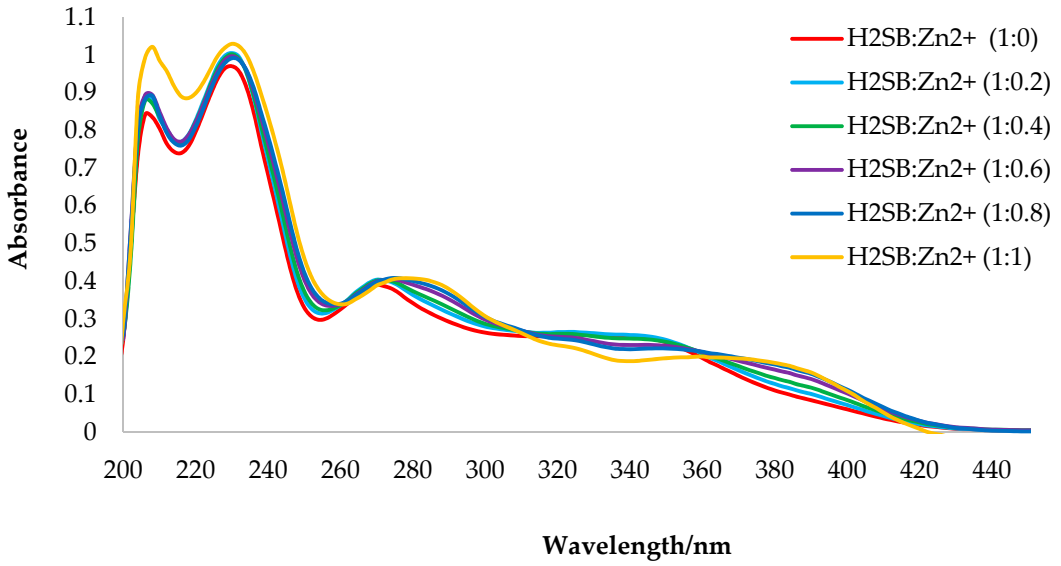

Figure S18. Absorption spectra of H_2SB (100 μM,) before (red line) and after addition of Zn^{2+} (100 μM), measured in methanol-water in 80:20 v/v (without the addition of pH modifiers, pH 7.0 - 7.5). Spectral data were recorded after the addition of Zn^{2+} in increasing volume (0.0, 0.2, 0.4, 0.6, 0.8 and 1.0 mL) to H_2SB (1.0 mL) at room temperature.

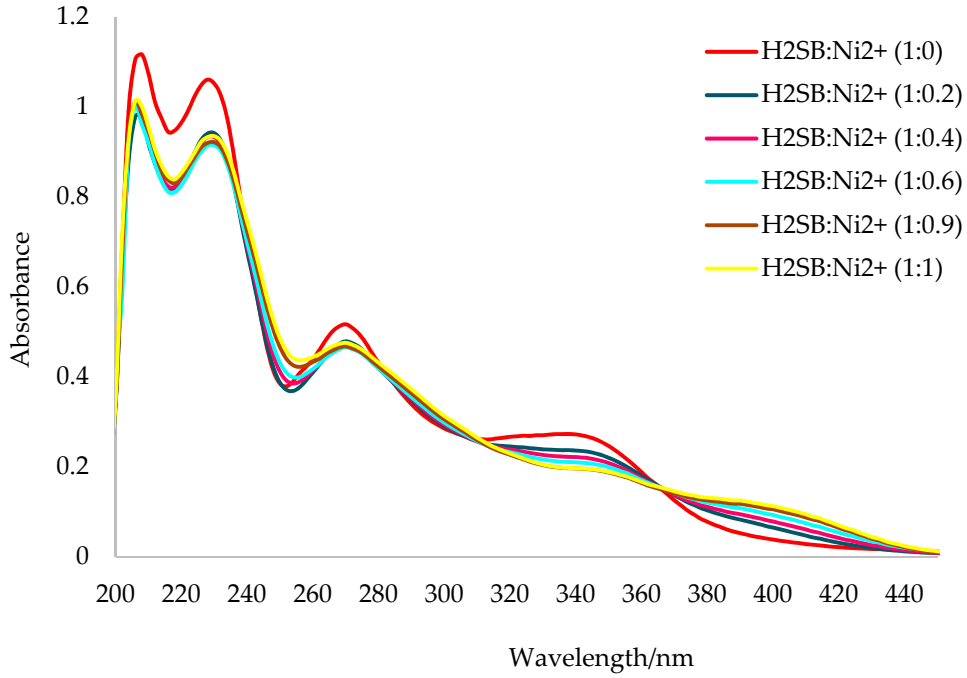

Figure S19. Absorption spectra of H_2SB (100 μM,) before (red line) and after addition of Ni^{2+} (100 μM), measured in methanol-water in 80:20 v/v (without the addition of pH modifiers, pH 7.0 - 7.5). Spectral data were recorded after the addition of Ni^{2+} in increasing volume (0.0, 0.2, 0.4, 0.6, 0.9 and 1.0 mL) to H_2SB (1.0 mL) at room temperature.

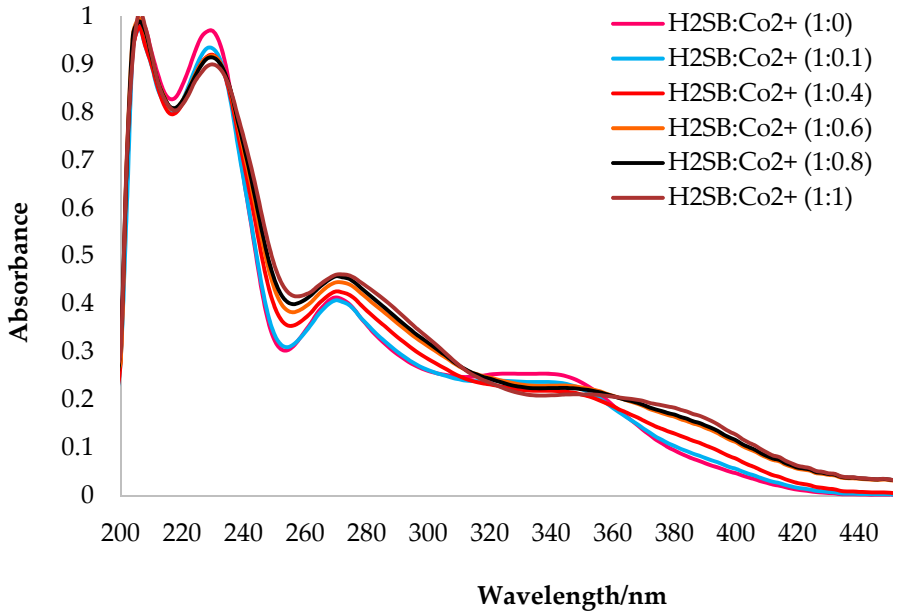

Figure S20. Absorption spectra of H_2SB (100 μM,) before (pink line) and after addition of Co^{2+} (100 μM), measured in methanol-water in 80:20 v/v (without the addition of pH modifiers, pH 7.0 - 7.5). Spectral data were recorded after the addition of Co^{2+} in increasing volume (0.0, 0.1, 0.4, 0.6, 0.8 and 1.0 mL) to H_2SB (1.0 mL) at room temperature.

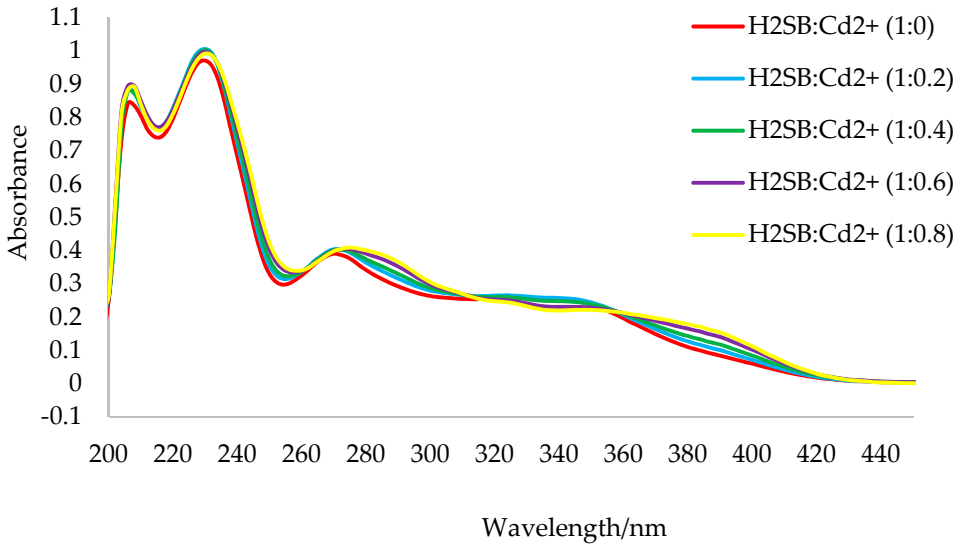

Figure S21. Absorption spectra of H_2SB (100 μM,) before (red line) and after addition of Cd^{2+} (100 μM), measured in methanol-water in 80:20 v/v (without the addition of pH modifiers, pH 7.0 - 7.5). Spectral data were recorded after the addition of Cd^{2+} in increasing volume (0.0, 0.4, 0.6 and 0.8 mL) to H_2SB (1.0 mL) at room temperature.

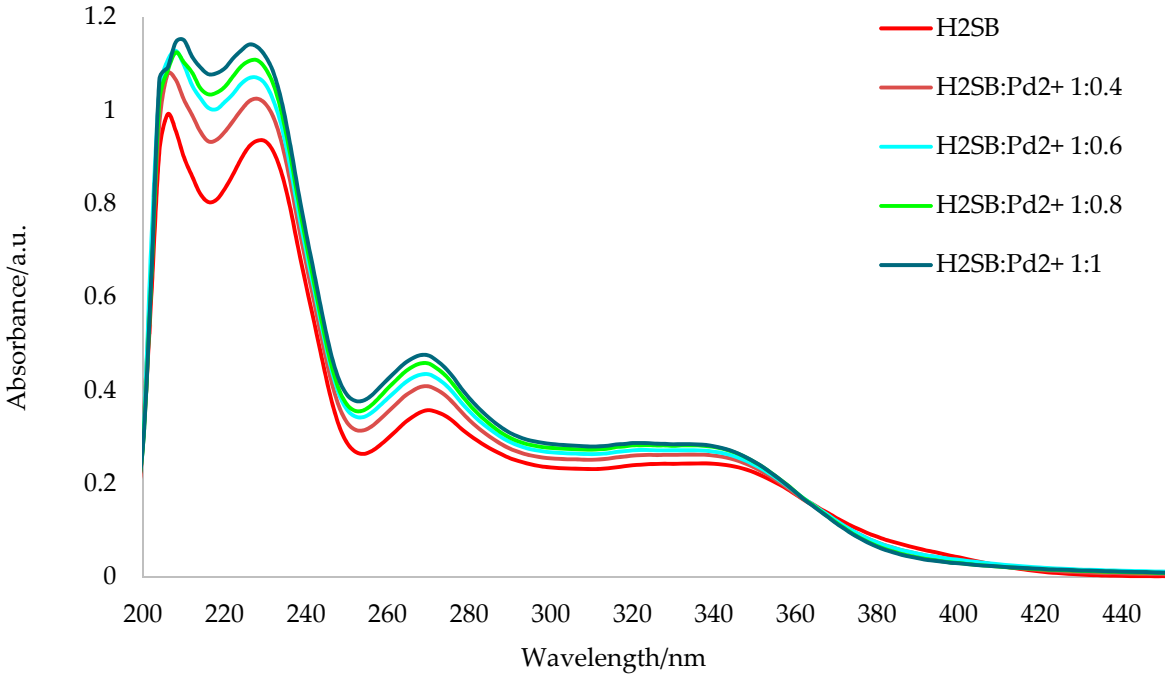

Figure S22. Absorption spectra of H_2SB (100 μM,) before (red line) and after addition of Pd^{2+} (100 μM), measured in methanol-water in 80:20 v/v (without the addition of pH modifiers, pH 7.0 - 7.5). Spectral data were recorded after the addition of Pd^{2+} in increasing volume (0.0, 0.4, 0.6, 0.8 and 1.0 mL) to H_2SB (1.0 mL) at room temperature.

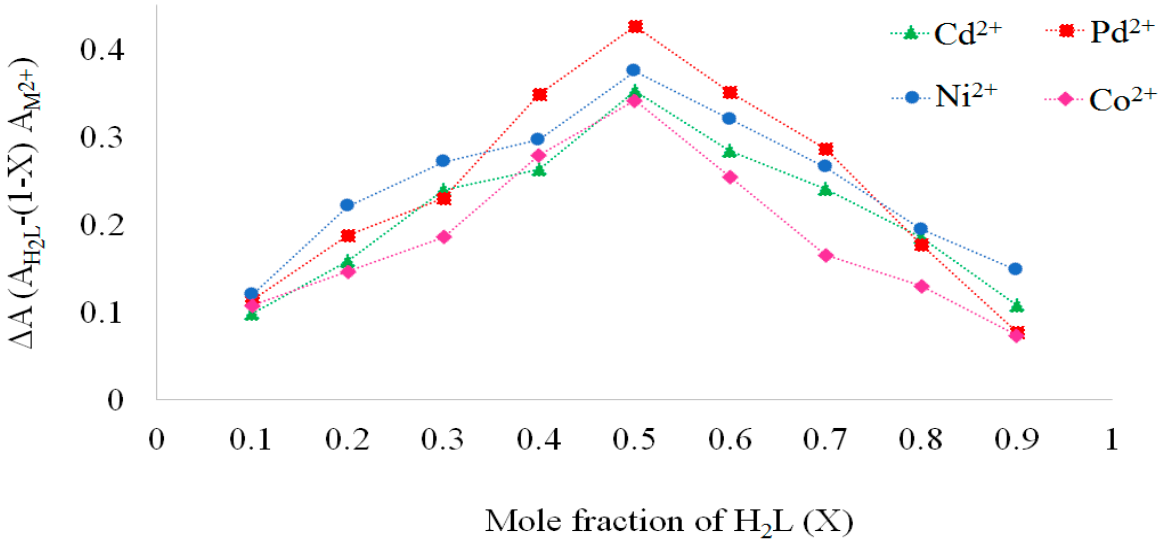

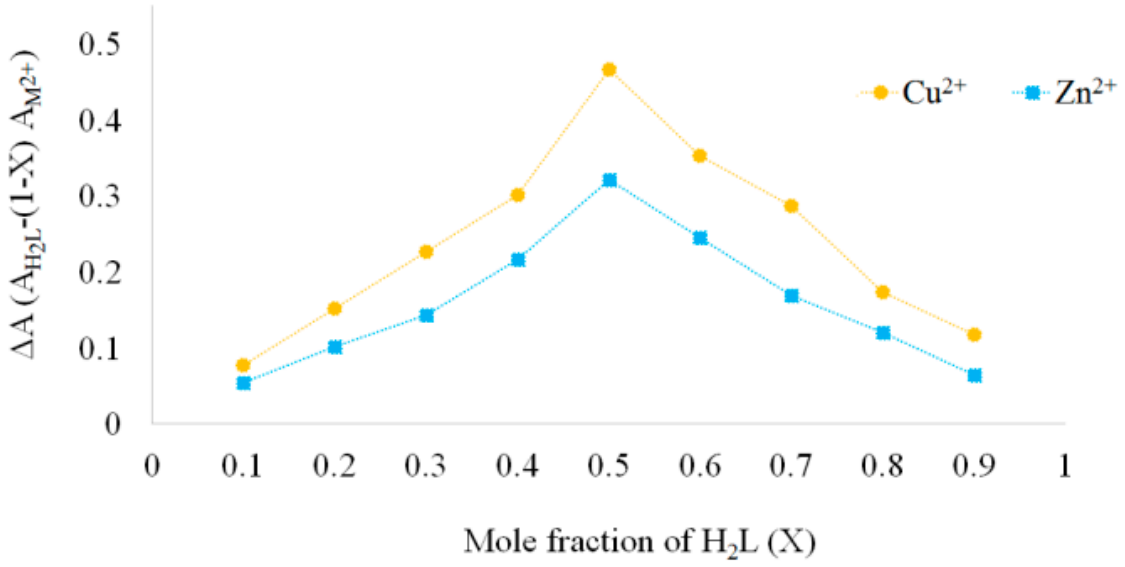

Figure S23. Job's plots for the determination of the binding stoichiometry of H2SB with Cu^{2+}, Zn^{2+}, Co^{2+}, Ni^{2+}, Cd^{2+} and Pd^{2+}.

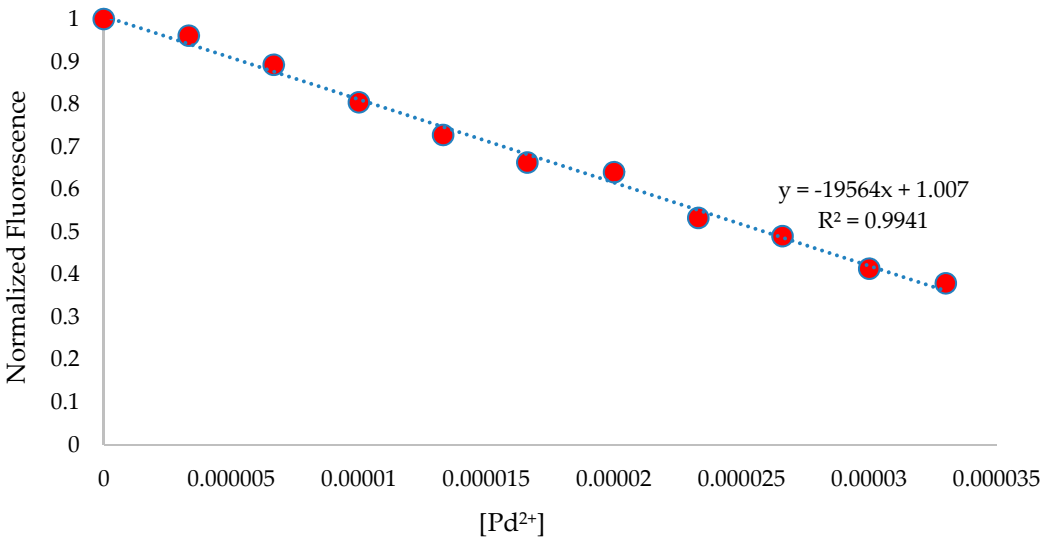

Figure S24. The linear relationship between fluorescence intensity and Pd^{2+} concentrations measured in methanol (pH 7.0-7.5) under λ_{exc} = 390 nm. Fluorescence intensity data have been rescaled to have values between 0 and 1. Spectral data were recorded at 5 minutes after the addition of Pd^{2+} (0.0, 0.1, 0.2, 0.3, 0.4, 0.5, 0.6, 0.7, 0.8, 0.9 and 1.0 mL) to H_2SB (1.0 mL) at room temperature.

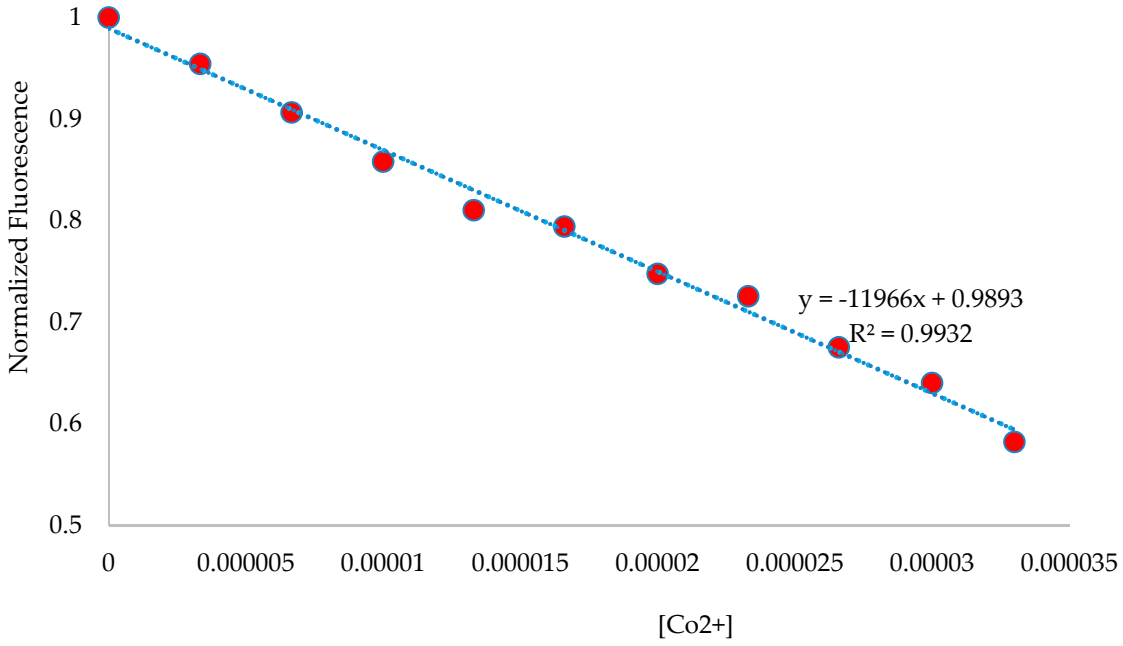

Figure S25. The linear relationship between fluorescence intensity and Co^{2+} concentrations measured in methanol (pH 7.0-7.5) under λ_{exc} = 390 nm. Fluorescence intensity data have been rescaled to have values between 0 and 1. Spectral data were recorded at 5 minutes after the addition of Co^{2+} (0.0, 0.1, 0.2, 0.3, 0.4, 0.5, 0.6, 0.7, 0.8, 0.9 and 1.0 mL) to H_2SB (1.0 mL) at room temperature.

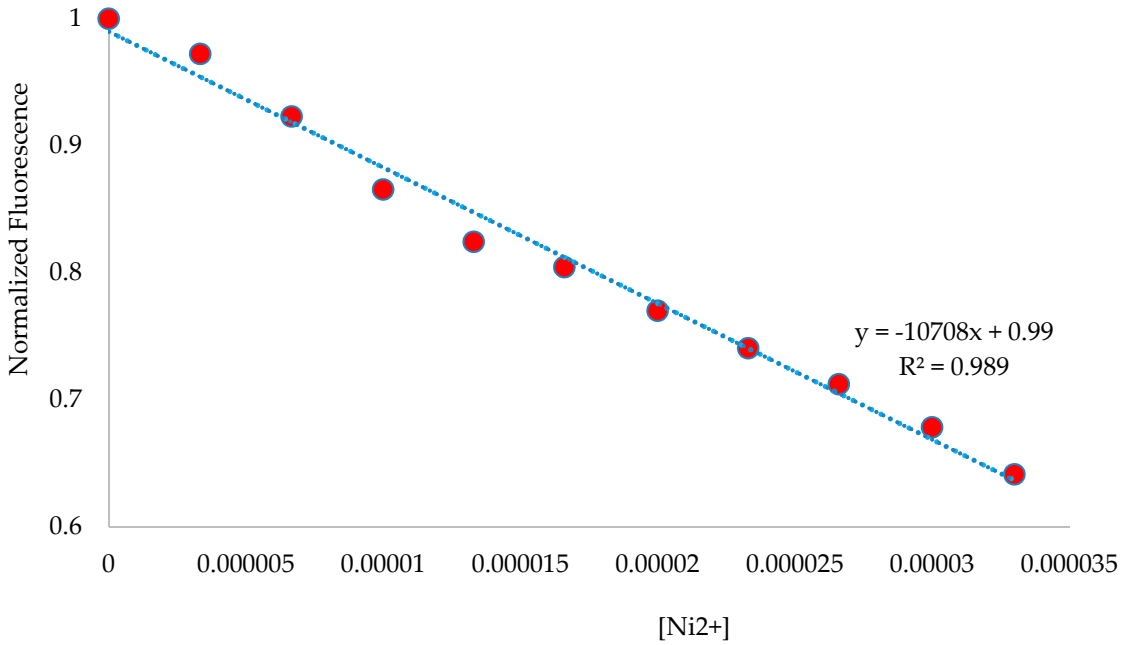

Figure S26. The linear relationship between fluorescence intensity and Ni^{2+} concentrations measured in methanol (pH 7.0-7.5) under λ_{exc} = 390 nm. Fluorescence intensity data have been rescaled to have values

between 0 and 1. Spectral data were recorded at 5 minutes after the addition of Ni^{2+} (0.0, 0.1, 0.2, 0.3, 0.4, 0.5, 0.6, 0.7, 0.8, 0.9 and 1.0 mL) to H_2SB (1.0 mL) at room temperature.

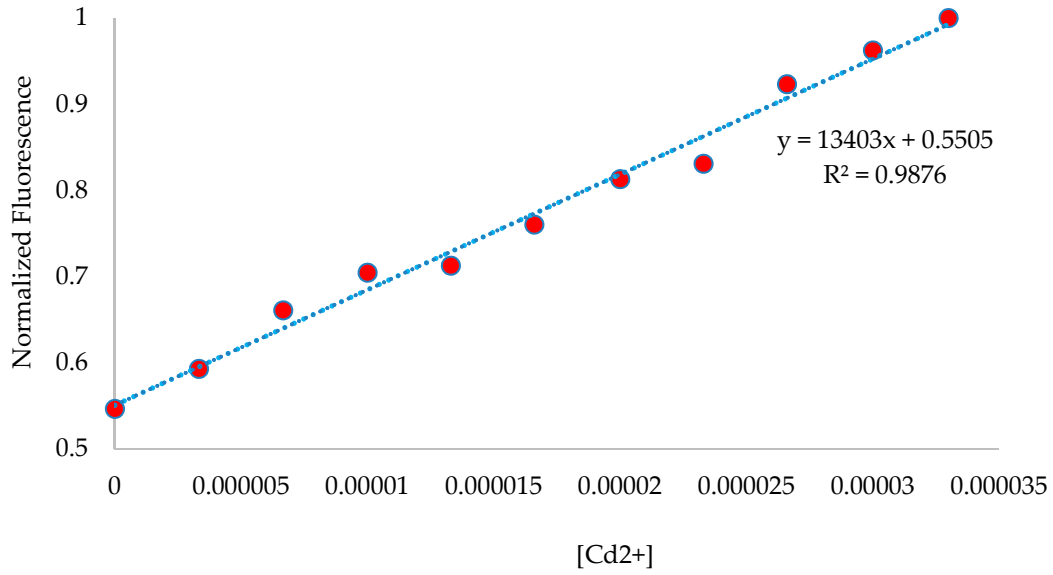

Figure S27. The linear relationship between fluorescence intensity and Cd^{2+} concentrations measured in methanol (pH 7.0-7.5) under λ_{exc} = 390 nm. Fluorescence intensity data have been rescaled to have values between 0 and 1. Spectral data were recorded at 5 minutes after the addition of Cd^{2+} (0.0, 0.1, 0.2, 0.3, 0.4, 0.5, 0.6, 0.7, 0.8, 0.9 and 1.0 mL) to H_2SB (1.0 mL) at room temperature.

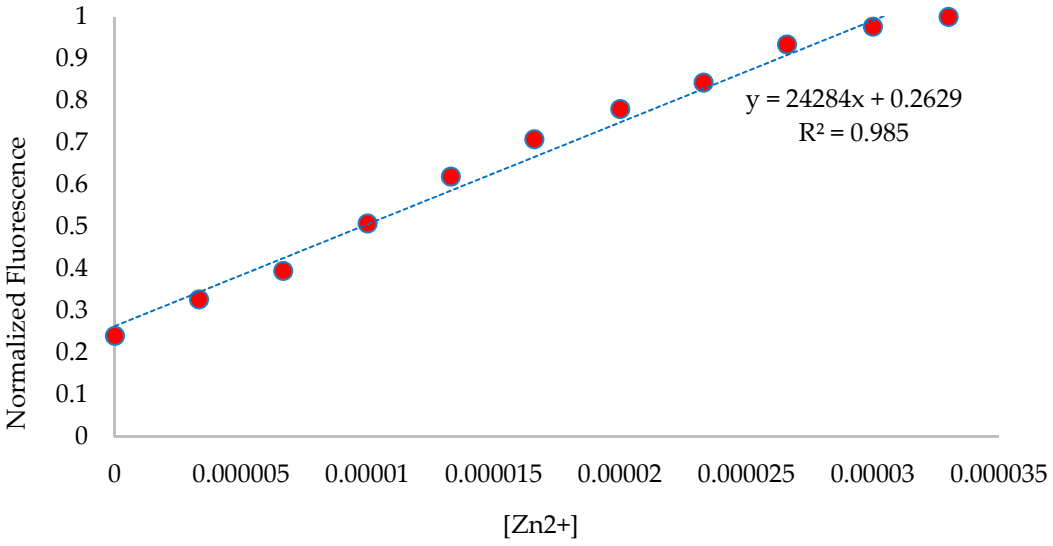

Figure S28. The linear relationship between fluorescence intensity and Zn^{2+} concentrations measured in methanol (pH 7.0-7.5) under λ_{exc} = 390 nm. Fluorescence intensity data have been rescaled to have values

between 0 and 1. Spectral data were recorded at 5 minutes after the addition of Zn^{2+} (0.0, 0.1, 0.2, 0.3, 0.4, 0.5, 0.6, 0.7, 0.8, 0.9 and 1.0 mL) to H_2SB (1.0 mL) at room temperature.

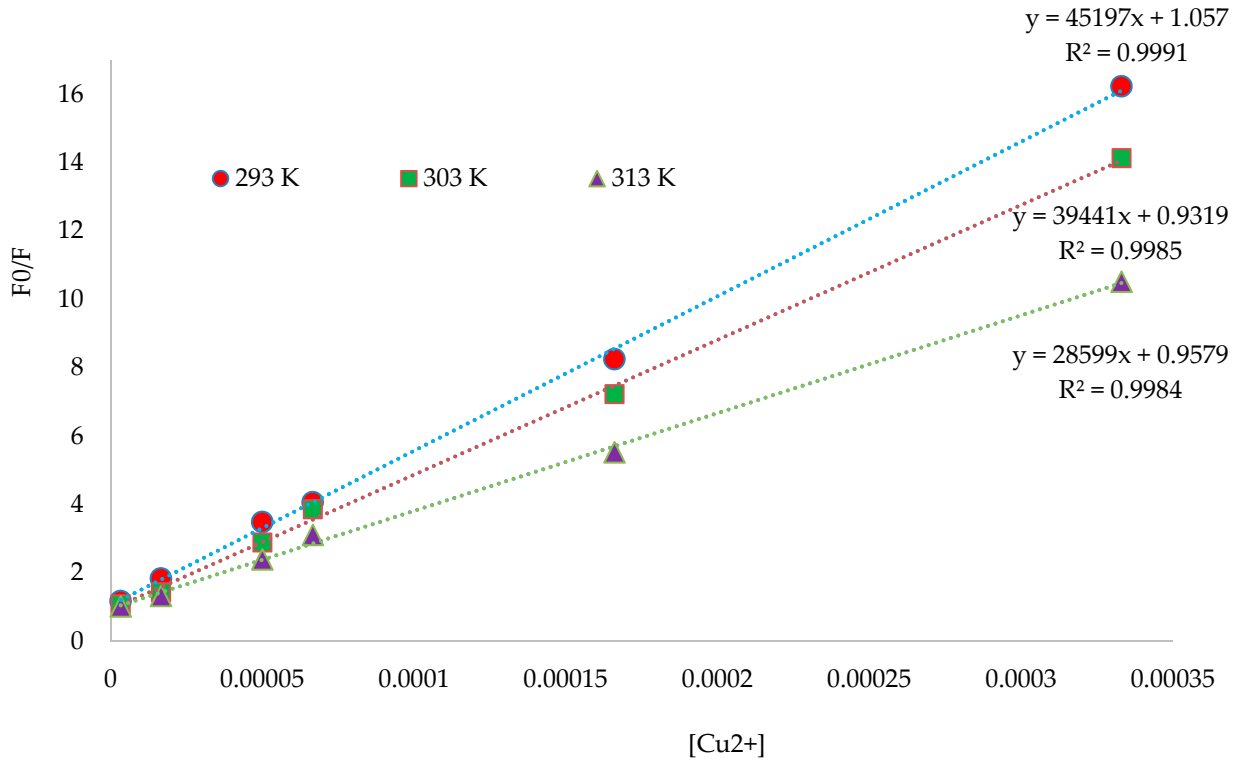

Figure S29. Plots of the intensities of the fluorescence spectra *vs* the concentration of the quencher. Slopes of the curves at 293, 303 and 313K are Stern-Volmer constants K_{SV} at the cited temperatures

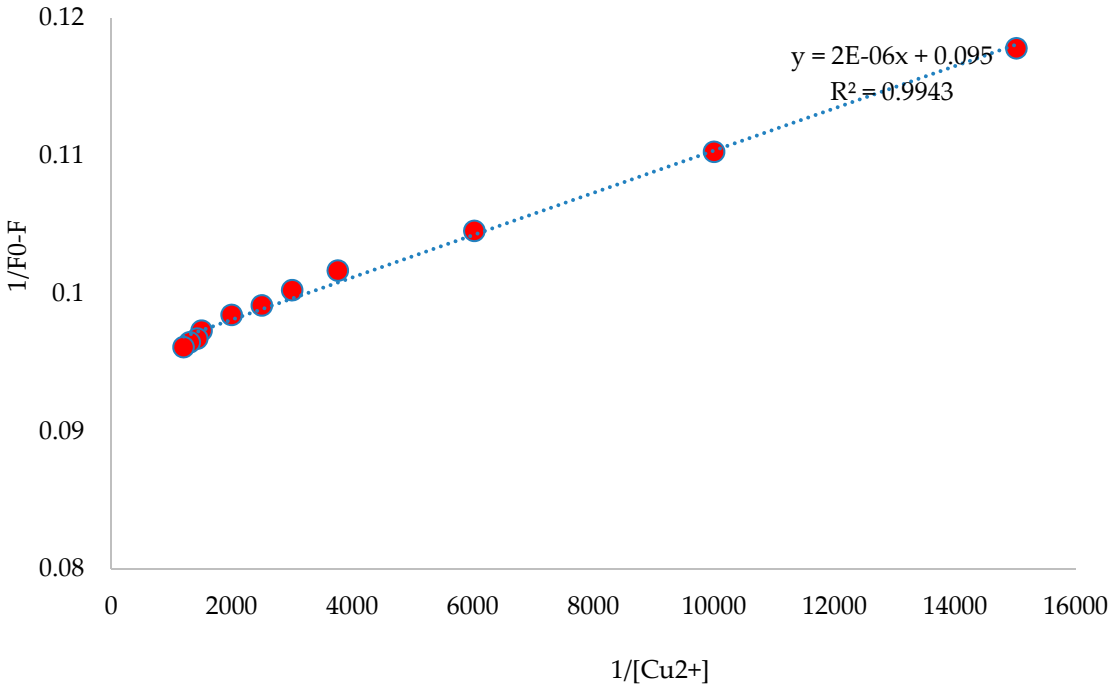

Figure S30. Benesi–Hildebrand plot from fluorescence titration data of H_2SB (100 μM) with Cu^{2+}. K_b = 47,500

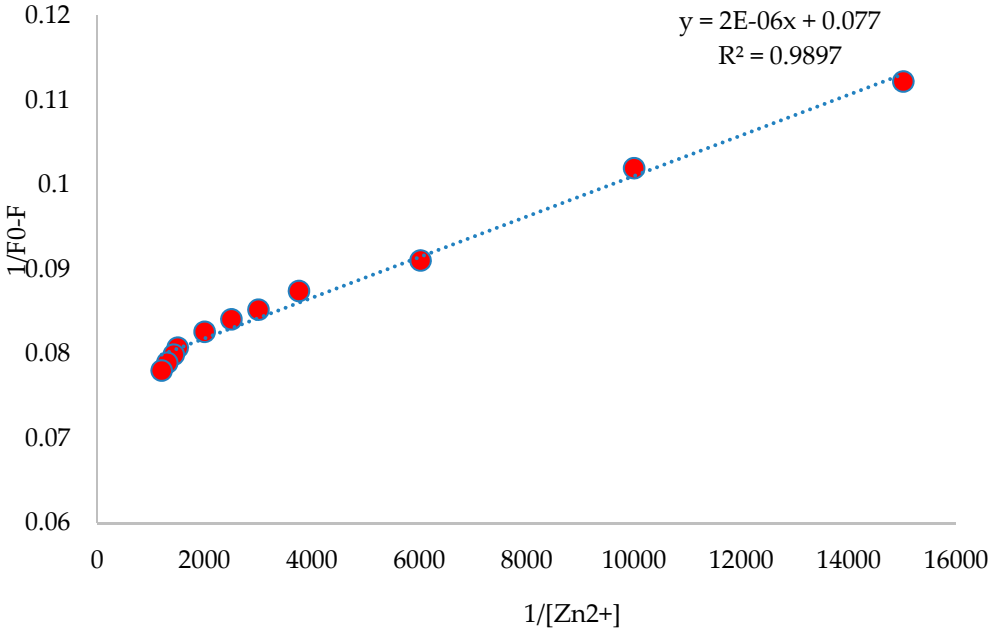

Figure S31. Benesi–Hildebrand plot from fluorescence titration data of H_2SB (100 μM) with Zn^{2+}. K_b = 38,500

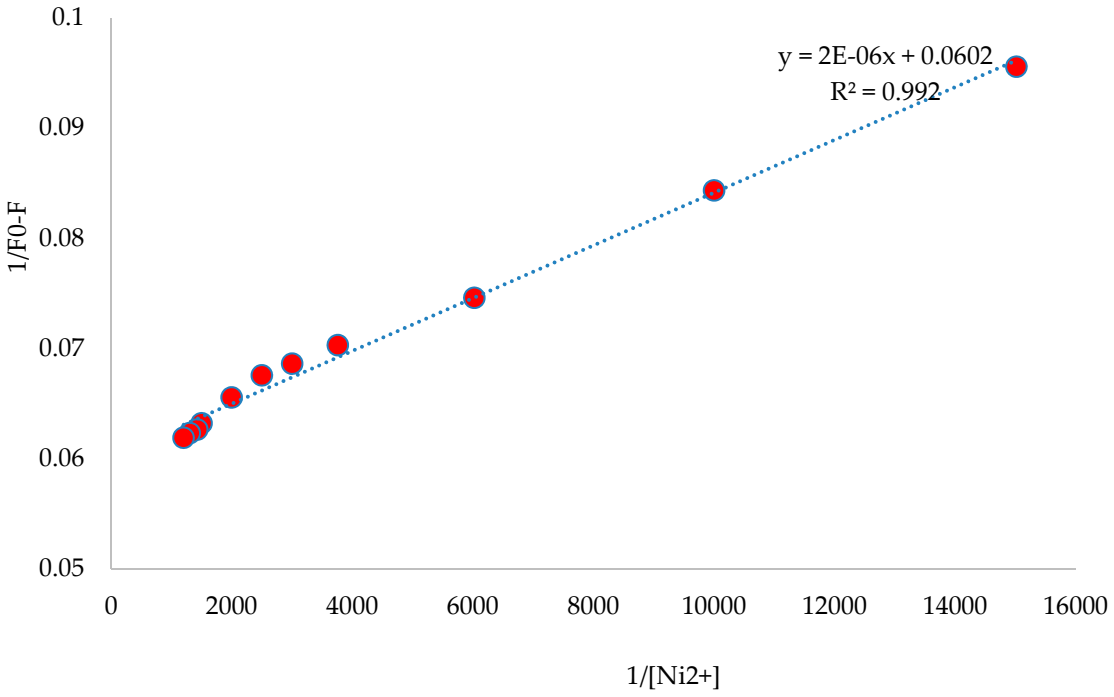

Figure S32. Benesi–Hildebrand plot from fluorescence titration data of H_2SB (100 μM) with Ni^{2+}. K_b = 30,100

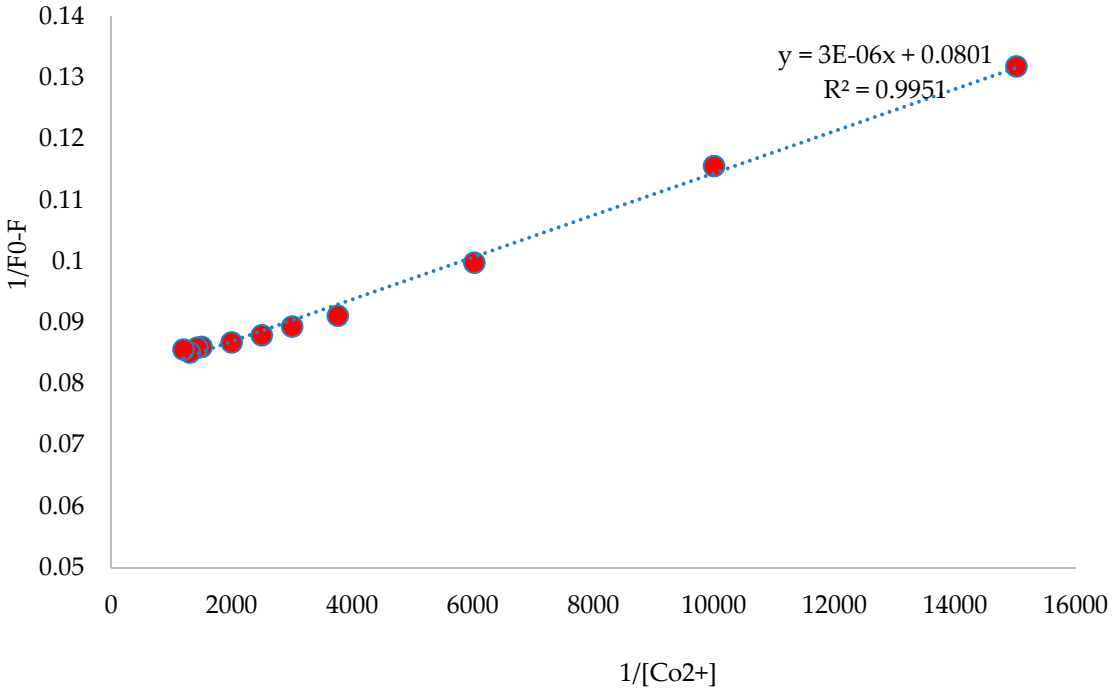

Figure S33. Benesi–Hildebrand plot from fluorescence titration data of H_2SB (100 μM) with Co^{2+}. K_b = 26,700

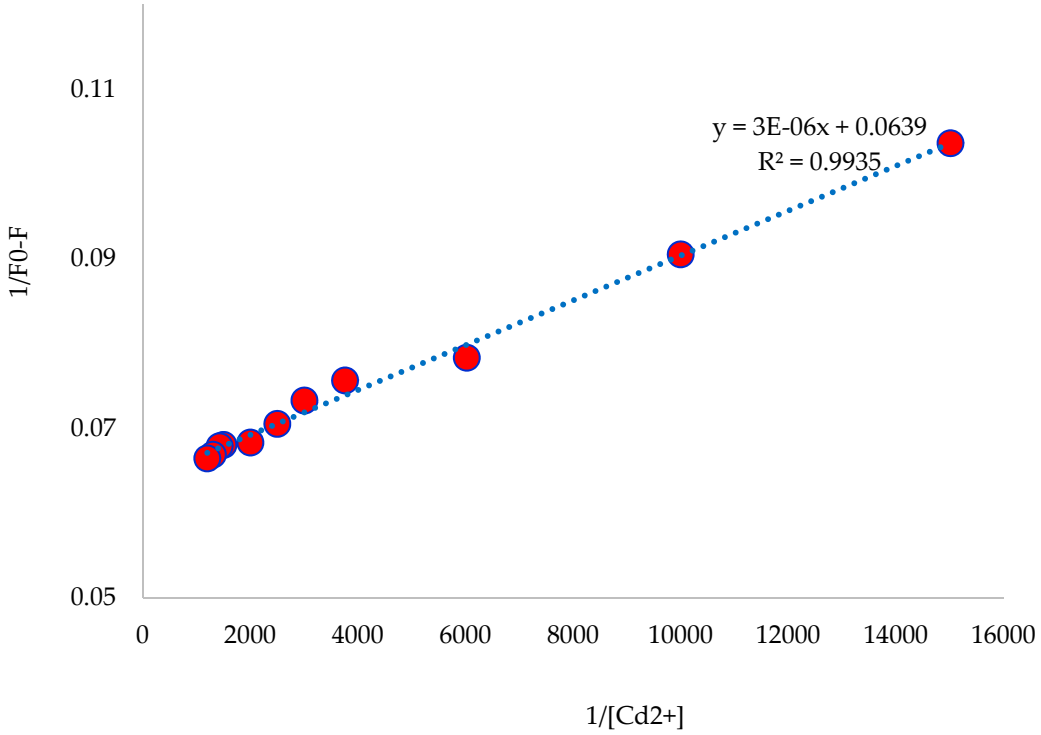

Figure S34. Benesi–Hildebrand plot from fluorescence titration data of H_2SB (100 μM) with Cd^{2+}. K_b = 21,300

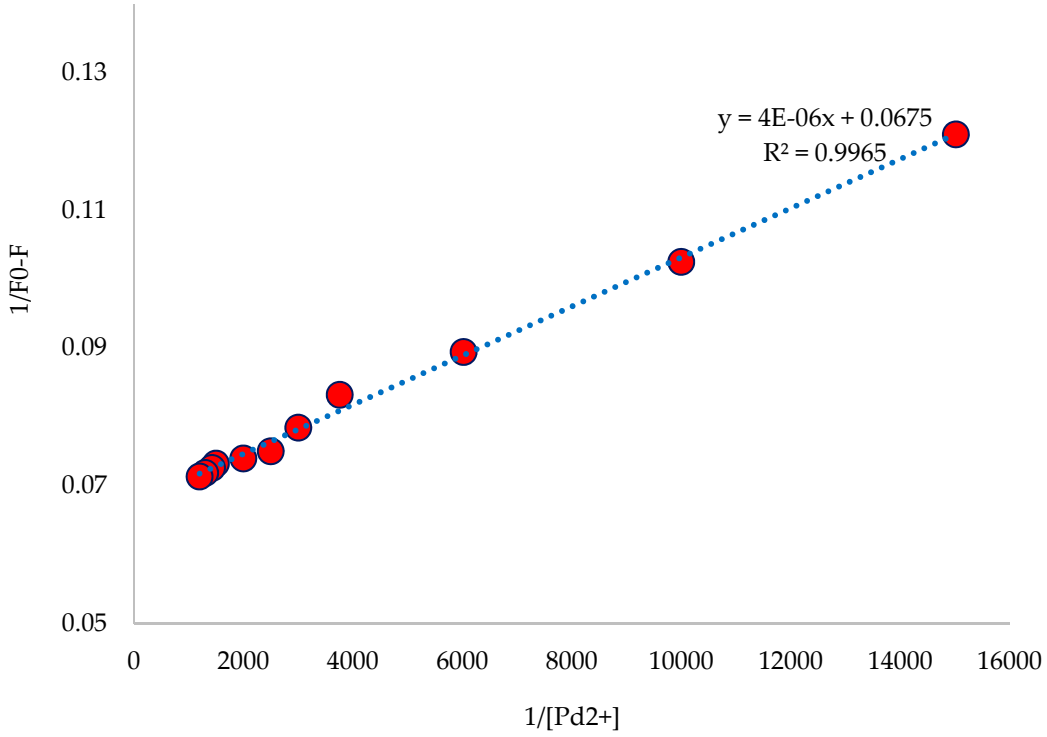

Figure S35. Benesi–Hildebrand plot from fluorescence titration data of H_2SB (100 μM) with Pd^{2+}. K_b =16,875.

Table S6. Figures of merits of some of the most recently reported fluorescent probes for Cu^{2+} ion determination.

Operation mode	$\lambda_{ex}/\lambda_{em}$ (nm)	LOD (μM)	Working range (μM)	Interference	Reference
Turn-OFF	390/500	0.083	0.276-33	None	Our work
Turn-OFF	394/498	0.0087	0.029-33	None	24
Turn ON	234/463	ND	ND	Fe^{2+}	38
Turn ON	365/485	0.2	0.2-20	None	39
Turn ON	401/513	ND	0.001-0.026	None	40
Turn ON	454/585	0.0087	ND	None	41
Turn OFF	350/396	2.20	4.72-59.84	None	42
Turn-OFF	355/438	10	ND	Ascorbic acid	43
Turn ON	424/472	0.00041	ND	None	44
Turn OFF	330/420	0.023	ND	Fe^{2+}	45
Turn ON	419/524	13.05	15-90	None	46
Turn OFF	570/635	0.124	ND	None	47
Turn-OFF	442/458, 567	0.1	ND	None	48
Turn-OFF	290/470	0.46	ND	None	49
Turn-OFF	270/482	3.98	1-63.1	Pb^{2+}	50
Turn-OFF	364/420	4.87	ND	None	51
Turn-ON	365/475	43.11	ND	Zn^{2+}	52
Turn-OFF	310/410	10	50-300	None	53
Turn-OFF	365/405	0.36	ND	Hg^{2+}	54
Turn ON	380/480	1.09	ND	Hg^{2+}	55
	400/505	1.19	ND	Hg^{2+}	
Turn ON	556/??	0.0431	10-220	None	56
Turn OFF	405/529	ND	2-5	None	57
Turn ON	521/559	0.912	ND	None	58
Turn OFF	290/405	0.92	ND	None	59
Turn OFF	290/405	0.96	ND	None	59
Turn ON	ND/600	0.26	ND	Co^{2+}, Fe^{3+}	60
Turn ON	467/574	0.82	ND	None	61
Turn ON	510/575	0.28	0.4-10	None	62
Turn OFF	240/361	ND	ND	Fe^{2+}	63
Turn OFF	340/512	0.44	ND	None	64
Turn OFF	ND/475	0.35	0-7	None	65
Turn ON	ND/423	0.676	ND	None	66

ND: Not disclosed